Materials Horizons

ROYAL SOCIETY OF CHEMISTRY

REVIEW

View Article Online
View Journal | View Issue

Published on 29 November 2023. Downloaded by West Lake University on 2/18/2024 5:45:26 PM.

Cite this: *Mater. Horiz.*, 2024, **11**, 626

Recent progress on defect-engineering in ferroelectric HfO_2: The next step forward *via* multiscale structural optimization

Fengjun Yan,[a] Yao Wu,[a] Yilong Liu,[a] Pu Ai,[a] Shi Liu,[b] Shiqing Deng,[c] Kan-Hao Xue,[a] Qiuyun Fu[ad] and Wen Dong*[ad]

Received 10th August 2023,
Accepted 22nd November 2023

DOI: 10.1039/d3mh01273e

rsc.li/materials-horizons

The discovery of unconventional scale-free ferroelectricity in HfO_2-based fluorite thin films has attracted great attention in recent years for their promising applications in low-power logic and nonvolatile memories. The ferroelectricity of HfO_2 is intrinsically originated from the widely accepted ferroelectric metastable orthorhombic $Pca2_1$ phase. In the last decade, defect-doping/solid solution has shown excellent prospects in enhancing and stabilizing the ferroelectricity *via* isovalent or aliovalent defect-engineering. Here, the recent advances in defect-engineered HfO_2-based ferroelectrics are first reviewed, including progress in mono-ionic doping and mixed ion-doping. Then, the defect-lattice correlation, the point-defect promoted phase transition kinetics, and the interface-engineered dynamic behaviour of oxygen vacancy are summarized. In addition, thin film preparation and ion bombardment doping are summarized. Finally, the outlook and challenges are discussed. A multiscale structural optimization approach is suggested for further property optimization. This article not only covers an overview of the state-of-art advances of defects in fluorite ferroelectrics, but also future prospects that may inspire their further property-optimization *via* defect-engineering.

Wider impact

Novel scale-free ferroelectrics in fluorite metal oxides have attracted much attention due to its unconventional ferroelectric origin, compatibility with CMOS technology, and robust remnant polarization. HfO_2-based ferroelectrics show distinct ferroelectricity from the metastable polar phase compared with conventional ferroelectrics. More importantly, doping and oxygen vacancies are vital in the formation of ferroelectric metastable phases. Sophisticated doping defects can generally induce/enhance the ferroelectricity of HfO_2 films *via* trivalent or tetravalent ion doping or solid solution, including Si, Al, Gd, La, Sc, Y, Zr, and Ce. Further development of the HfO_2-based ferroelectric memories should face challenges from the stable control of the ferroelectric metastable phase, coercive field, wake-up and fatigue effects. Defect-engineering would be vital to provide a promising way to solve these challenges and requires more attention. Currently, a review discussing the correlation between lattice atoms, point defects, interfacial defects and ferroelectric polarization at different structural scales is still missing. We found that defects on a different structural scale would distinctly affect the ferroelectric performance. We thus suggest that it is necessary to understand/build the coupling law of an atomic lattice, defect dipole, ferroelectric domain, heterogenous interface, and ferroelectric polarization in order to overcome these challenges.

1 Introduction

Electronic devices based on ferroelectric (FE) thin films have been of interest to the research community for decades. Ferroelectric devices are widely used in ferroelectric memories, piezoelectric sensors, infrared detectors and other fields because of their important properties such as ferroelectricity, piezoelectricity and pyroelectricity.[1–3] Traditional perovskite ferroelectric materials, such as Pb(Zr, Ti)O_3 (PZT), $BaTiO_3$ (BTO) and $SrBi_2Ta_2O_9$ (SBT), to be used in ferroelectric memories, have reached a dilemma in terms of their incompatibility with CMOS processes[4] and size effect since the ferroelectric

[a] School of Integrated Circuits & Wuhan National Laboratory for Optoelectronics & Engineering Research Center for Functional Ceramics of the Ministry of Education, Huazhong University of Science and Technology, Wuhan 430074, China. E-mail: dongw@hust.edu.cn; Tel: +0086-15871392972
[b] Key Laboratory for Quantum Materials of Zhejiang Province & Department of Physics, University of Electronic Science and Technology of China, Chengdu 611731, China
[c] Beijing Advanced Innovation Center for Materials Genome Engineering, Institute for Advanced Materials and Technology, University of Science and Technology Beijing, Beijing 100083, China
[d] Shenzhen Huazhong University of Science and Technology Research Institute, Shenzhen 518000, P. R. China

This journal is © The Royal Society of Chemistry 2024

Published on 29 November 2023. Downloaded by West Lake University on 2/18/2024 5:45:26 PM.

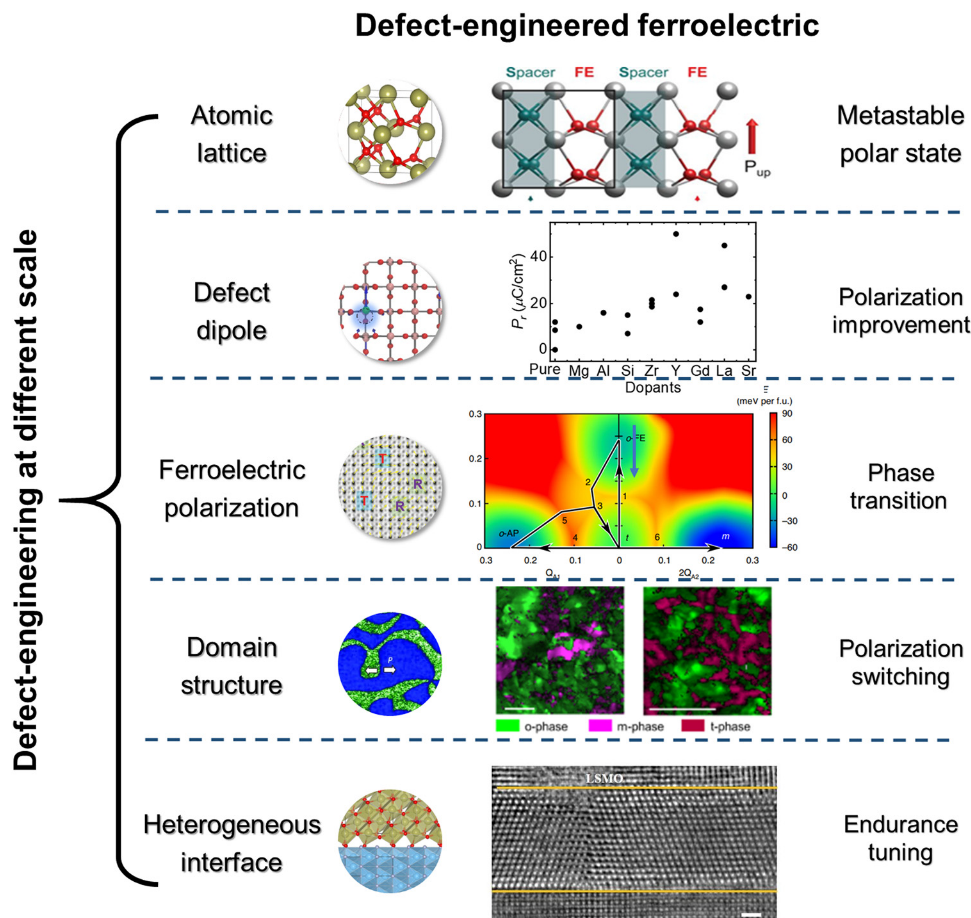

Fig. 1 The recent progress in defect-engineered ferroelectric HfO_2 from various aspects. The lattice structure of the o-phase.[7] Mapping of reported typical maximum remnant polarization values in pure and doped fluorite-based metal oxides MO_2 (M = Zr, and Hf) with different dopants.[8] Energy landscape of bulk HfO_2 as a function of the amplitudes of three different lattice modes.[9] The green, magenta, and red colors represent the o-, m-, and t-phase regions, respectively.[10] The STEM image of the domains (mutually rotated by 180° about [111]) in the r-phase.[11]

performance degrades sharply at thicknesses less than 70 nm.[5,6] The exploration of non-perovskite ferroelectric thin films has become a potential breakthrough point. Fig. 1 below illustrates the progress of multifaceted research on defect-engineered ferroelectric HfO_2.

In 2011, T. S. Böscke *et al.*[12] found the ferroelectricity in non-centrosymmetric orthorhombic hafnium oxide (HfO_2) thin film materials prepared by atomic layer deposition (ALD), and silicon-doped HfO_2 also exhibit good ferroelectricity. The novel ferroelectrics in fluorite metal oxides have attracted much attention due to their compatibility with CMOS technology[6,13] and robust remnant polarization with no size effect at the nanoscale ($\sim$50 μC cm^{-2}),[14–17] which is significantly higher than that of BTO ($\sim$26 μC cm^{-2}).[18] Moreover, the low synthesis temperature, good thermal stability and corrosion resistance,[19] higher coercive field[20] and much slower ferroelectric domain moving[21] expand the applications in electronic devices.

However, HfO_2-based ferroelectrics show distinct ferroelectricity compared with conventional ferroelectrics. From the aspect of phase structures, there are eight polymorphous phases (Fig. 2) in HfO_2-based thin films reported both experimentally and theoretically, including the room temperature monoclinic (m) $P2_1/c$ phase (the only stable phase in most reports), high temperature tetragonal (t) $P4_2/nmc$ (a parent phase of $Pca2_1$ and $P2_1/c$) and cubic (c) $Fm\bar{3}m$ phase (highly centrosymmetric), high pressure fluorite CaF_2-type antipolar phase, and disordered orthorhombic (o) *Pbcm* phase, and cotunnite ($PbCl_2$)-type *Pmnb* phase.[9] It is widely accepted that their ferroelectricity originates from a metastable polar orthogonal phase $Pca2_1$[26–28] rather than the $Pmn2_1$ phase,[27,29] and an epitaxially-engineered rhombohedra phase like (r) *R*3 or *R*3*m* has also been found through experiments and theoretical calculations.[26,30–32] Additionally, an antiferroelectric phase called *Pbca*,[33] and another nonpolar *Pbca* phase exists only under high pressure.[25] These confusions and uncertainties stem from the multiphase structural properties of HfO_2 and the complexity in its nanoscale characters. Recently, the discovery of scale-free ferroelectricity[34] and flat polar phonon band[7] has greatly advanced the understanding of the ferroelectricity in HfO_2 from an average structure, which fundamentally explains the distinct polarization origin and higher coercive field. The scale-free ferroelectricity would enable high-density

Published on 29 November 2023. Downloaded by West Lake University on 2/18/2024 5:45:26 PM.

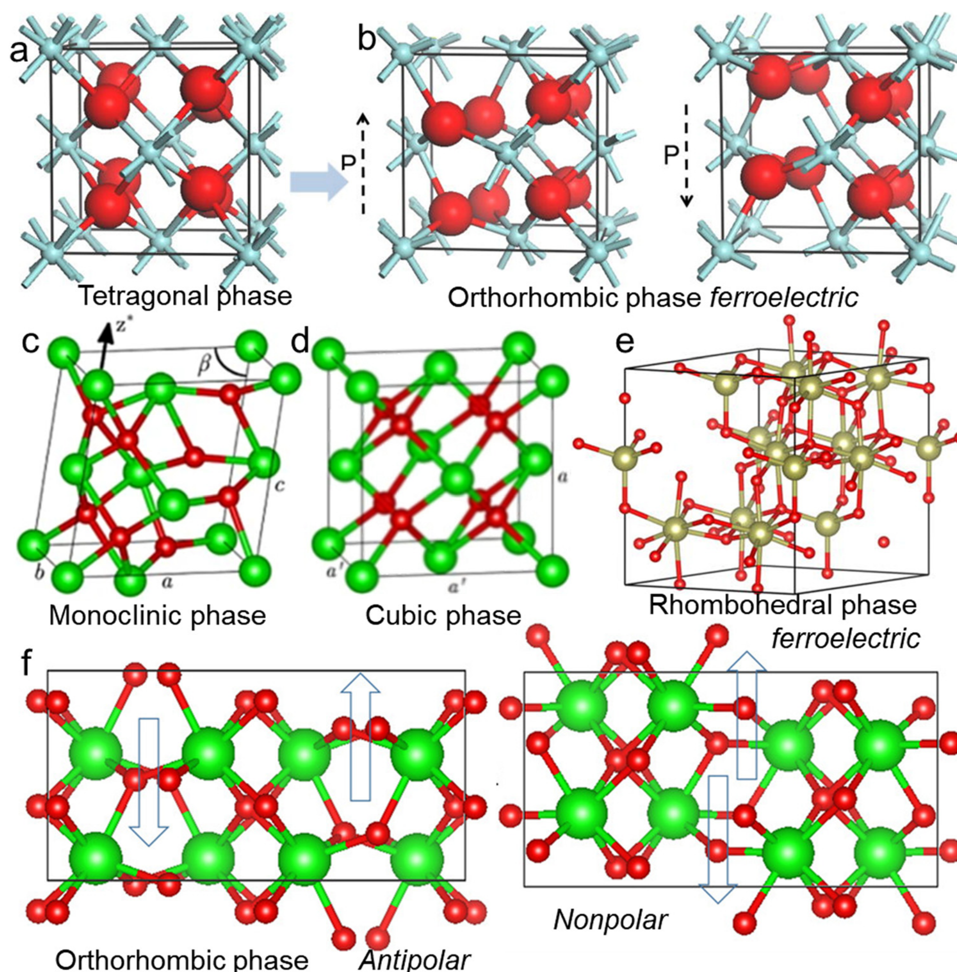

Fig. 2 Schematic structure of unit cells of various polycrystalline types. (a) $P4_2/nmc$, two different polarization states of (b) $Pca2_1$,[22] (c) $P2_1/c$,[22] (d) $Fm\bar{3}m$,[23] (e) $R3m$,[24] and (f) $Pbca$ of antipolar and nonpolar nature.[25]

information memory applications. More importantly, doping,[20,35–38] deposition substrates,[39,40] covered electrodes,[12] internal stress,[41,42] oxygen vacancies,[43,44] surface energy[23] and electric fields[20] will all affect the formation and stability of its ferroelectric metastable phase, remanent polarization, coercive field, wake-up and fatigue effects and other ferroelectric behaviors.

From previous analysis, unlike the traditional perovskite ferroelectrics, doping and oxygen vacancies play a very important role in the formation of ferroelectric metastable phases in HfO_2-based thin films. Sophisticated doping defects can generally induce/enhance HfO_2 films *via* trivalent or tetravalent ion doping or solid solution, including Si,[45] Al,[46] Gd,[47] La,[48] Sc,[49] Y,[9] Zr,[16] and Ce.[36] In 2021, Xu *et al.*[9] reported that ferroelectric metastable phase $Pca2_1$ and antiferroelectric phase $Pbca$ were formed in Y-doped HfO_2 single crystals. Theoretical calculations show that Y-doping plays a key role in the formation of the ferroelectric metastable phase, but there is a lack of in-depth analysis and research on defects. From a material level point of view, further development for applications of the HfO_2-based ferroelectric memories should face challenges in stability control of the ferroelectric metastable phase, lowering the coercive field, and wake-up and fatigue effects, and defect-engineering would be vital to provide a promising way to solve these challenges.

There have been numerous review articles discussing the ferroelectricity in HfO_2-based systems,[50–52] while the correlation between lattice atoms, point defects, interfacial defects and ferroelectric polarization is still missing. To address the various issues on the progress of the defects in HfO_2-based ferroelectrics, we summarized the state-of-art studies on the defect doping engineering in this novel material system. In this article, we focus on the defect-engineering in HfO_2. Currently, most research studies mainly focus on mono ion doping. Among all the defect-modulated ferroelectric properties, the thermodynamics of oxygen vacancy is vital to kinetically stabilize the metastable orthorhombic phase and promote the phase transition. Meanwhile, mono ion doping (*i.e.* Sc, Al) is vital to control the oxygen vacancies due to charge balance, and research into the mixed ion-co-doping is expected in the future for its ability to enhance endurance. Moreover, we show that ionic doping can also introduce local distortion and modulate a

 This journal is © The Royal Society of Chemistry 2024

Published on 29 November 2023. Downloaded by West Lake University on 2/18/2024 5:45:26 PM.

polar phonon band. Based on this review, we suggest that in order to understand the correlation between defects and ferroelectricity, it is necessary to understand/build the coupling law of atomic lattice, defect dipole, ferroelectric domain, heterogenous interface, and ferroelectric polarization. We hope this article will encourage the readers to re-consider the optimization strategy of HfO_2-based ferroelectrics and provide guidance on how to take advantage of point-defects to improve the HfO_2-based information storage devices.

2 Ferroelectric origin in HfO_2

Since the discovery of the ferroelectricity in Si doped HfO_2, endeavors have been made to understand the unconventional ferroelectricity origin and optimize the ferroelectric properties of the fluorite structure. Most works report films grown by atomic layer deposition which are polycrystalline and contain multiple phases (m-phase, t-phase and o-phase *etc.*). It is well recognized that the ferroelectricity of HfO_2 originates from the ferroelectric metastable phase in terms of average structure. Currently, it has been demonstrated that among HfO_2-ZrO_2-based thin films, orthorhombic $Pca2_1$ ($Pbc2_1$ in some references)[12,26–28] and rhombohedral $R3m$[26,30–32] phases also exhibit ferroelectric behavior in recent studies. The former is widely accepted by researchers and the latter was recently found is some special situations like under large strain and stress, high concentration doping and even an unbalanced Hf/Zr–O ratio.

2.1 Orthorhombic phase

The polar orthorhombic phase ($Pca2_1$, o-phase) was first reported for Mg-doped ZrO_2 when cooled to cryogenic temperatures.[53] This polar phase is widely considered to be the origin of the recently reported structures based on the ferroelectric HfO_2 thin films and there are also a large number of experimental and theoretical studies.[26,38,54–56] Among all potential fluorite crystal structures, the orthorhombic ferroelectric (o-FE) phase is the most commonly accepted one to give rise to ferroelectricity.

To verify the o-FE phase, Xu *et al.*[9] used a neutron diffraction pattern combined with refinement to determine the phase and lattice parameters of 12% HfO_2:Y single crystal. The observed diffraction intensities in Fig. 3a are reliably fitted by the 100% o-FE orthorhombic phase with lattice parameters of a = 5.1019 Å, and b = 5.154 Å (Fig. 3a). Fig. 3b shows the calculated energy landscape of bulk HfO_2 as a function of the amplitudes of several characteristic modes corresponding to the stable or metastable t, m, o-AP, and o-FE phases based on density functional theory calculations. High-angle annular dark-field (HAADF)-STEM analysis displayed a strong contrast associated with the heavy Hf atoms. Both the o-FE phases with a boundary along $[100]/[001]_{\text{o-FE}}$ can be directly observed, showing irregularly shaped *ab* and *bc* twin domains and a curved domain wall.[9]

To better visually characterize both the crystal orientation and phase information with high spatial resolution ($\sim$2 nm), Lee *et al.*[10] used a TEM precession electron diffraction (PED) technique for two-dimensional mapping (Fig. 3e). As shown in Fig. 3f–g, for a $\sim$4 nm thick film, the two-dimensional mapping image shows a mixture of $\sim$80% o-phase and $\sim$20% m-phase. While, Fig. 3h–i show the formation of a mixed phase of 65% o-phase and $\sim$35% t-phase, in which the nonpolar m-phase is suppressed in $\sim$2 nm thick film. This indicates that the increased surface energy at reduced dimension prefers the formation of the t-phase, as the present phase of the o-phase, which have a lower surface energy than the m-phase. These results from both theoretical and experimental analysis suggest the formation of a metastable o-FE phase gives rise to the ferroelectricity in the polymorphic nature of the HfO_2-based fluorite system.

2.2 Rhombohedral phase

In addition to an orthorhombic ferroelectric phase, a rhombohedral phase has also been determined in the abraded surfaces layer under the stress of partially stabilized zirconia,[57] However, no electrical properties were reported in these studies. As shown in Fig. 4a–d, the rhombohedral phase was obtained on epitaxial $Hf_{0.5}Zr_{0.5}O_2$ films grown on $SrTiO_3$ (STO) by Wei *et al.*[57] Both the high energy rhombohedral (r-) phase ($R3m$ or $R3$) and spontaneous polarization (P_s = 34 μC cm^{-2}) were observed in the HfO_2-ZrO_2 system, but at the same time the films showed greater coercivity than the polar o-phase. The internal pressure of the nanoparticles induced by the large surface energy and the compressive strain exerted by the substrate, are suggested to work together to stabilize the r-phase.[31] The presence of the rhombohedral phase was later seen in HZO epitaxial films[58] and HfO_2–Sc_2O_3 solid solutions films[59] grown on silicon where lattice distortion also shows the stabilizing effect of compressive strain on the r-phase.

In addition, in conjunction with the structure of the r-phase shown by experimental observations, Zhang *et al.*[30] also derived the result from theoretical calculations that under in-plane compressive strain (Fig. 4e and f), the [111]-oriented $R3m$ phase exhibits a vertical long and short Hf–O bonding order, which is important for the origin of the ferroelectricity. The $R3m$ phase HfO_2 films leading to the emergence of ferroelectricity are stabilized by the combined effect of size and strain.

However, a recent experiment in the $R3m$ phase showed another possibility for achieving stable ferroelectricity in HfO_2-based thin films. Wang *et al.*[32] discovered rhombohedral ferroelectric $Hf(Zr)_{1+x}O_2$ rich in hafnium–zirconium [Hf(Zr)], which means a higher ratio of Hf/Zr–O. The unbalanced Hf/Zr–O ratio expands the lattice and increases the lattice stresses, which stabilize both the rhombohedral phase (r-phase) and its ferroelectricity. It seems that the lattice strain and stress originated from the unbalanced Hf/Zr–O ratio play a critical role in stabilizing the r-phase, but there are still few studies on this and more efforts are required.

Although recent studies have shown much evidence on the r-phase, there are still numerous problems that ought to be explored such as the stabilization mechanism and the

Published on 29 November 2023. Downloaded by West Lake University on 2/18/2024 5:45:26 PM.

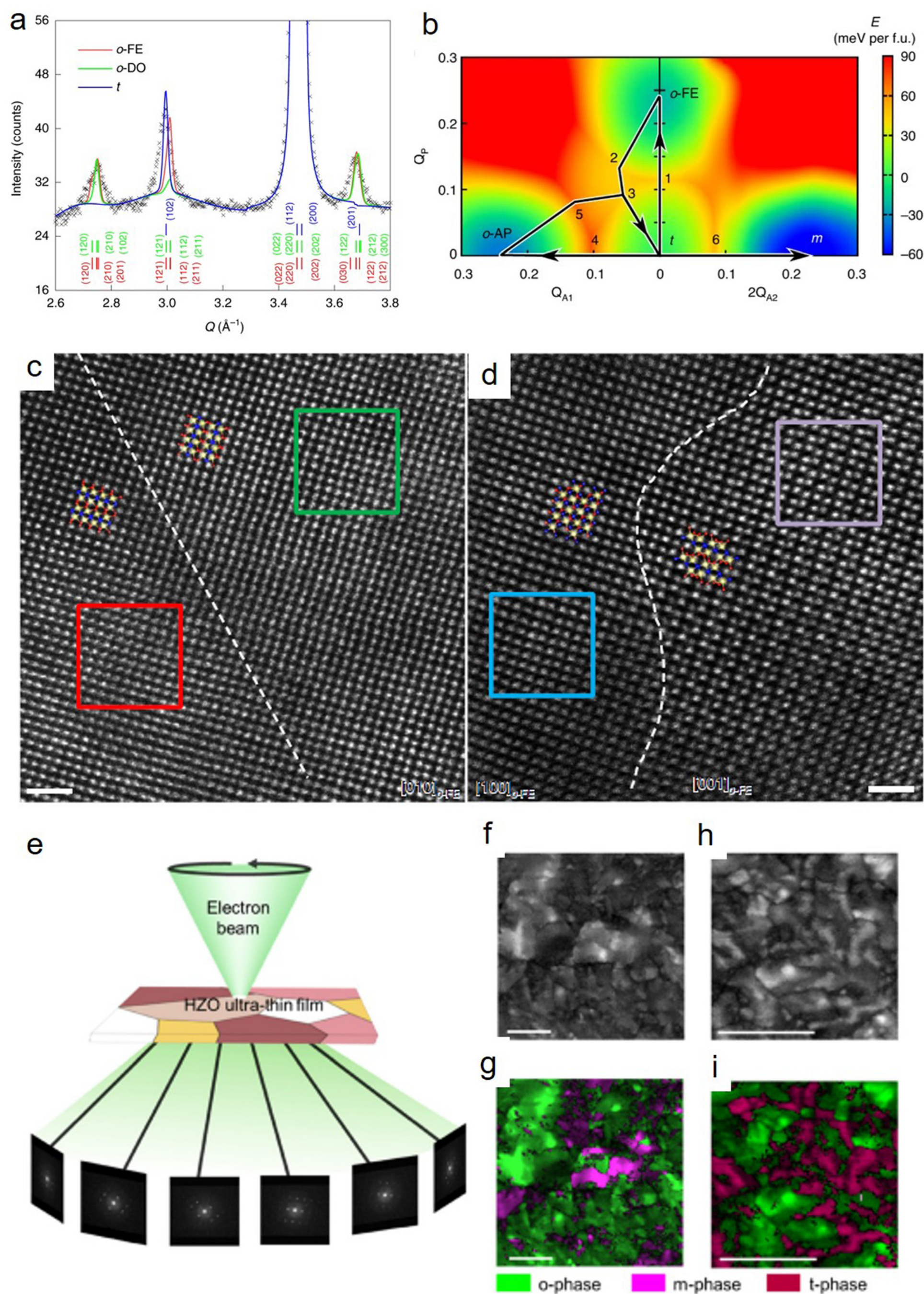

Fig. 3 (a) A representative neutron diffraction pattern against momentum transfer Q (Å^{-1}) to reveal the o-FE phase of the 12% Y doped HfO_2 single crystal. (b) Energy landscape of bulk HfO_2 as a function of the amplitudes of three different lattice modes. Here, Q_P is the amplitude of a polar mode, and Q_{A1} and Q_{A2} are the amplitudes of two different antipolar modes. (c) and (d) HAADF-STEM image along [100]/[001]$_{o\text{-FE}}$, showing irregularly shaped ab and *bc* twin domains and the curved domain wall. The domain walls indicated with dashed lines are added as a guide to the eye. The o-FE models are superimposed (Hf, yellow; O, blue and red). Scale bar, 1 nm.[9] (e) Schematic of the TEM PED technique. (d)–(f) Index maps and (e)–(g) corresponding phase distribution maps for (f) and (g) 4- and (h) and (i) 2-nm-thick HZO films obtained through TEM PED measurements. In panels (g) and (i), the green, magenta, and red colors represent the o-, m-, and t-phase regions, respectively. The scale bars in panels (d)–(g) represent 100 nm.[10]

ferroelectricity origin of the r-phase, and how a lower wake-up effect, better coercive field and high endurance are realized.

2.3 Polarization switching mechanism

To realize ferroelectricity, a double-well potential should exist in hafnium-based ferroelectrics, which means a feasible ferroelectric polarization switching. Therefore, the polarization switching mechanism cannot be avoided on the way to understanding the ferroelectricity origin. As typical ion-displacement ferroelectrics, polarization switching mainly relies on the shifting of polar O atoms for HfO_2 and its variants under external stimuli such as an electric field. However, the switching

 This journal is © The Royal Society of Chemistry 2024

Published on 29 November 2023. Downloaded by West Lake University on 2/18/2024 5:45:26 PM.

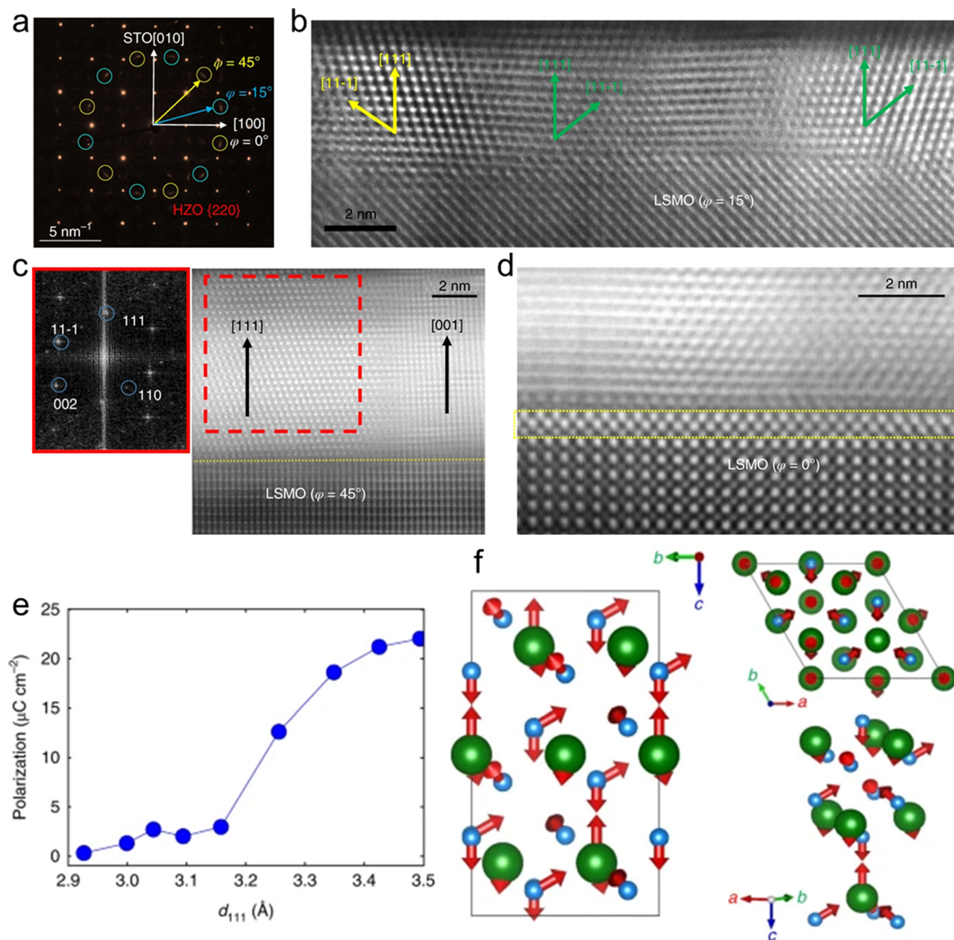

Fig. 4 (a) Plane-view SAED pattern from a 9-nm-thick HZO sample. (b) Cross-sectional HAADF-STEM image (corrected for sample drift) of the 9-nm-thick HZO film, observed along the [110] zone of the substrate (φ = 45°). Inset (left): Fourier transform of the [111] domain. (c) Representative cross-sectional HAADF-STEM image (drift-corrected) of a 4-nm-thick film, observed along the zone axis defined by φ = 15°. (d) HAADF-STEM image observed along STO [100], revealing a clear interfacial t-phase of HZO. (e) Computed polarization of the *R*3*m* phase of HZO as a function of d_{111}. (f) Two views of the *R*3*m* phase obtained for epitaxially compressed HZO and HfO_2 and detailed view of the Hf/Zr–O groups that characterize the *R*3*m* structure. Green (cyan) spheres represent Hf/Zr (O) atoms. The arrows show the polar distortion.[31]

mechanism is still under debate. Since the *Pca*2_1 and *Pmn*2_1 phase were suggested as the orthorhombic phase,[27] the ion-displacement of polarization switching in HfO_2 or ZrO_2 and their variants is widely studied.[55,60–63] Different pathways for uniform switching and opposite domain wall motion were also studied in our recent work.[64]

Currently, most studies are focused on the ferroelectricity in the ferroelectric phase of *Pca*2_1. Thus, the polarization switching mechanism on this metastable phase is discussed here. In 2014, the energy barrier of polarization switching was firstly calculated to around 0.4 eV using the NEB (nudged elastic band) method,[65] which opens up the way to understanding the atomic level evolutions of polarization switching, but the conventional NEB method cannot precisely describe the solid state transitions, moreover, the pathway referring to 0.4 eV is not the only shifting choice for active O atoms. Unlike the perovskite materials, there are more than 2 ideal pathways on polarization switching which have been proved in different theoretical studies as shown in Fig. 5a and b.

However, these reports are mainly based on Hf/ZrO_2 or their variants, and little attention has been paid to explore the defect effects on the polarization switching mechanism. Moreover, the recently developed variable cell solid state NEB method fixed the deficiency of NEB in the solid state transition.[68] Recently, Silva *et al.*[67] reported a epitaxial orthorhombic phase in La doped HfO_2 films with a constantly decreasing coercive field for 2–5 at% La-doping and suggested that the reason is the defects of doping lower the energy barrier in different pathways of polarization switching in the domain wall as shown in Fig. 5c and d, and could lead to a large polarization value ($\sim$70 μC cm^{-2}). In general, the polarization switching pathways are very clear by slight shifting of the B atom in traditional perovskite ferroelectrics (such as ABO_3), but it is opposite in HfO_2 as a large movement of polar atoms will lead to different pathways divided to moving through the Hf atomic plane or not. This behavior will lead to a more sophisticated ferroelectric origin, especially under the defect effect.

Published on 29 November 2023. Downloaded by West Lake University on 2/18/2024 5:45:26 PM.

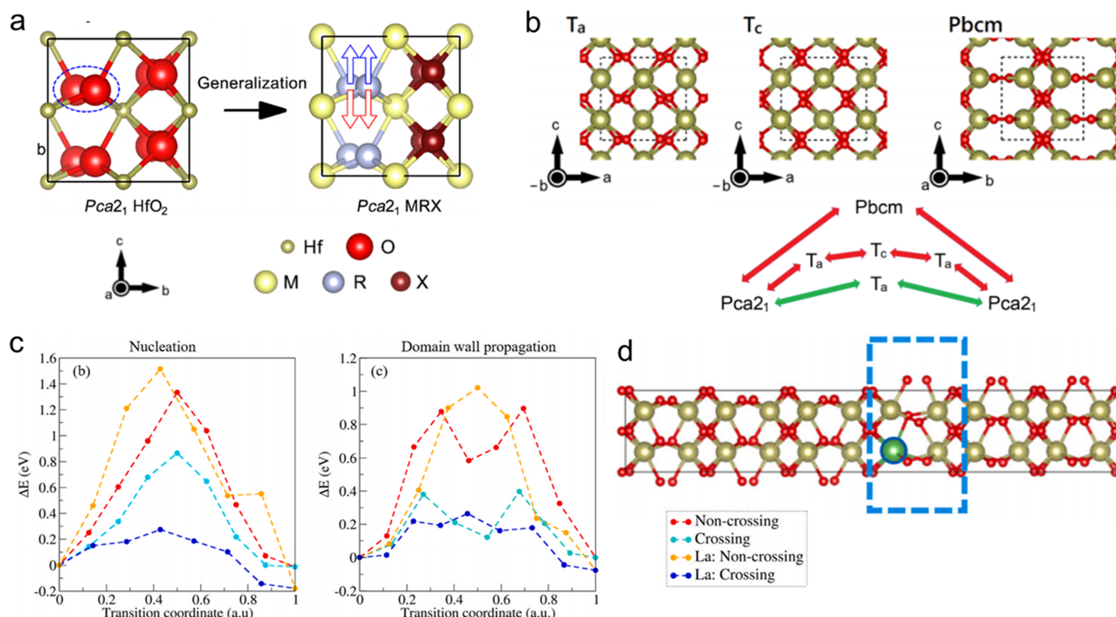

Fig. 5 (a) Crystal structures of orthorhombic $Pca2_1$ HfO_2 and their polarization relationships under the defects of MRX (M = Sr, Ta, Y; R = O, S, I; X = N, F, Br, I)[66] (b) The top panel is the transition states (including T_a and T_c, different variants of $P4_2/nmc$ and $Pbcm$) and the transition order of polarization switching in HfO_2.[62] (c) Comparison between La doped and undoped switching energy barriers for the crossing and non-crossing paths of a nucleation process. (d) Representation of the O/O interface in a La (green atom) doped 6 × 1 × 1 HfO_2 supercell. The distorted domain considered for the switching barrier calculation is highlighted by the blue dashed rectangle.[67]

So far, there are few studies on defect-induced polarization switching, but the defect engineering in hafnium-based ferroelectrics can be a next breakthrough for understanding the polarization origin of HfO_2. In addition, the polarization switching mechanism of the r-phase is still unclear and deserves more exploration.

2.4 Flat phonon band in fluorite ferroelectrics

Though the metastable ferroelectric phase gives rise to HfO_2-based ferroelectricity, its unique properties, such as a much higher coercivity and scale-free ferroelectricity, are still not clear at an atomic level. Using first-principal calculations, Lee *et al.*[7] found that the flat bands of polar phonons and consequent localized dipoles induce scale-free ferroelectric ordering in HfO_2 (Fig. 6). The flat bands of electrons, photons, and magnetic oscillators cause singular phenomena, but the flat polar phonon bands and their consequences in ferroelectrics are unknown. The appearance of flat phonon bands in HfO_2 explains the origin for its scale-free ferroelectricity. The unique flat polar phonon band with a periodic nonpolar/polar/nonpolar sandwich structure, gives rise to high coercivity and scale-free ferroelectricity.

As shown in Fig. 6a–e, the flat polar phonon bands induce stable independently switchable dipoles. The phonon dispersion in Fig. 6a indicates that the X_2' mode corresponding to the cubic structure is unstable due to the negative value of the mode frequency. Meanwhile, the modes at Γ_{15}^z and Y_5^z are stable and they condense in-phase with equal magnitude to generate an orthorhombic structure that consists of alternating spacer layers and ferroelectric layers with up (top) and down (bottom) polarization, respectively. The flat phonon in Fig. 6f shows the full phonon spectra of the HfO_2 where flat phonon bands in the vibration lattice mode are shown in the inset image. The polar and antipolar modes condensed in orthorhombic HfO_2, giving rise to periodic antipolar/polar/antipolar sandwich structures. As shown in Fig. 6g, the diagram demonstrates the reduction of symmetry from the cubic structure, where condensation of the main phonon modes (X_2', Γ_{15}^z, Y_5^z) transforms the cubic phase into a tetragonal structure, and the *z*-directional shift of the oxygen atoms in the phonon modes gives the structure a uniform polarization, driving it towards the orthorhombic phase and forming the dead layer. This differs from conventional ferroelectric materials in that the domain walls separating the 180° polar structural domains in $PbTiO_3$ are diffuse, wide and the polarization is suppressed in their vicinity. However, the elastic interactions between the HfO_2 ferroelectric domains are shielded by the spacer layer, which also explains the scale-free ferroelectricity in HfO_2 films with even sub-nanometer thickness. The zero-width domain is further indicated by the energy landscape in Fig. 6g. The emergence of flat phonon bands in HfO_2 provides a missing link to extend those exotic phenomena to ferroelectrics.

From the above results, we can see from both the experimental and theoretical results, the metastable orthorhombic $Pca2_1$ phase is mainly responsible for the appearance of ferroelectricity in HfO_2. While, by epitaxially growing the HfO_2 on a rhombohedral substrate, one can induce a rhombohedral phase in HfO_2 due to the interfacial proximity effect. However,

Published on 29 November 2023. Downloaded by West Lake University on 2/18/2024 5:45:26 PM.

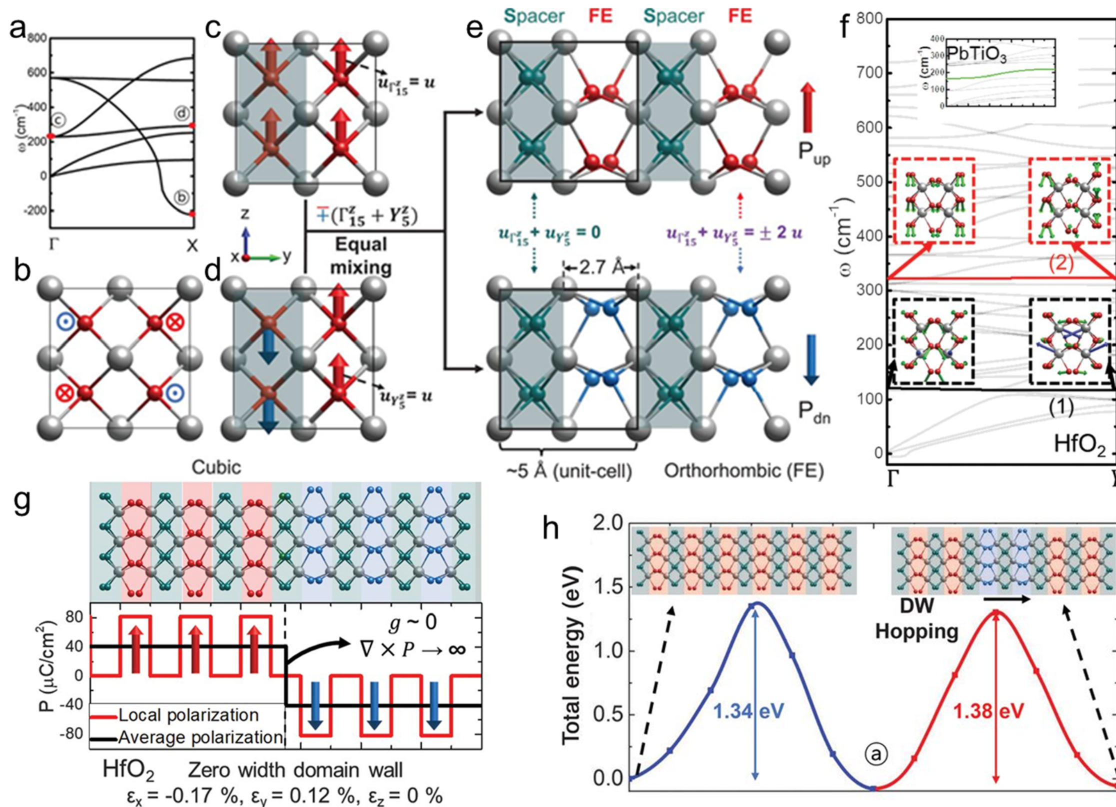

Fig. 6 In orthorhombic HfO_2: structural origin of alternating ferroelectric and nonpolar layers, flat-band and zero-width domain walls, and robust stability of wide ferroelectric domains in half-unit cells. (a) Phonon dispersion of the cubic phase. The red dots labeled b, c, and d denote the primary instability of (b) X_2' mode, (c) Γ_{15}^z, and (d) Y_5^z, respectively, where arrows denote u, the displacements of oxygen atoms. (e) Polar Γ_{15}^z and antipolar Y_5^z phonons condense in-phase with equal magnitude to generate an orthorhombic structure that consists of alternating spacer layers and ferroelectric layers with up (top), and down (bottom), polarization, respectively. Silver spheres indicate Hf atoms; red and blue spheres indicate oxygen atoms in the ferroelectric layer with up and down polarization, respectively; and green spheres indicate oxygen atoms belonging to the spacer layer. (f) This is because of its low energy cost ($g \sim 0$) guaranteed by the flatness of polar phonon bands involving the polar and antipolar modes condensed in orthorhombic HfO_2. Flat polar bands are indicated with black and red lines, and eigenmodes at Γ and Y in the bands are depicted in the insets. This flatness of the bands in HfO_2 is in sharp contrast to a dispersive band in $PbTiO_3$. (g) The atomic structure of the domain wall and variation in local polarization along the direction perpendicular to the domain walls in HfO_2. Red and black lines correspond to the local polarization averaged over their half- and single-unit cells, respectively. (h) Energy along the path of polarization switching of HfO_2, starting from the uniformly polarized structure to a state with reversed polarization in two layers.[7]

it is still not clear enough how the metastable ferroelectric phase can be stabilized. Considering the appearance of the ferroelectricity in HfO_2 is originally observed from Si doped HfO_2 and the metastable orthorhombic phase easily obtainable in doped HfO_2, the doping defect and its relation to ferroelectricity is thus another missing link to extend their unique phenomena to ferroelectricity origin.

3 Defect-modulated ferroelectricity

From the discovery of Si doped HfO_2 to rare earth element doped HfO_2 and to HZO solid solution, doping defects have been widely used to induce and improve the ferroelectricity in HfO_2-based ferroelectrics.[11,46] In this part, we will first review the literature about the mono-doping engineered ferroelectricity in doped HfO_2 and HZO solid solution. Then, the ferroelectric polarization dynamics associated with the defects will be summarized. Finally, the interface-assisted thermal dynamic behaviour of point defects will be presented to further understand the ferroelectric properties of HfO_2.

3.1 Mono-ionic doping

Since the earliest reports of the ferroelectric properties of Si-doped HfO_2, tremendous studies have reported the effects of different doping ions on the HfO_2-based ferroelectricity. As shown in Fig. 7, a periodic table is present with a solid element diagram to indicate the element that has been used. However, the mechanism of mono-ionic doping is still ambiguous to realize the ferroelectricity.

Fig. 8a shows the typical polarization hysteresis loops of the HfO_2 doped with different kinds of elements, including Zr, Si, Sr, Al, and rare earth elements (*i.e.* La, Y, Gd).[6] The P_r value of the doped HfO_2 first increases as the doping level increases and generally reaches its maximum at a critical doping level (Fig. 8b). For Ge and Zr doping, a much higher doping concentration is required.[6] Sangita *et al.* suggest that small

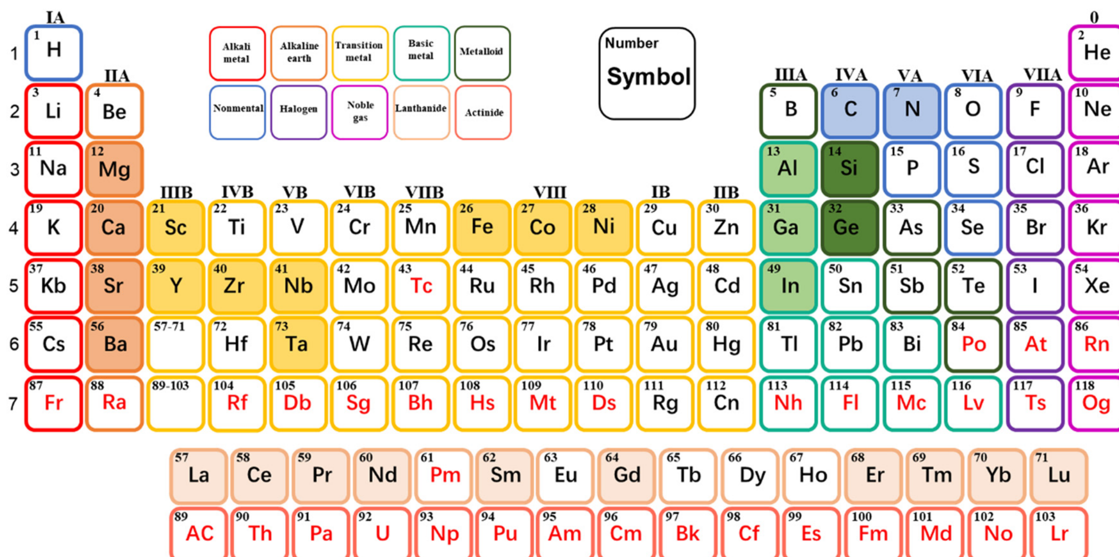

Fig. 7 Elements that have been shown to induce ferroelectricity in HfO_2 in the laboratory (red for radioactive elements). A solid element diagram indicates that the element has been used to dope the HfO_2 system.

Published on 29 November 2023. Downloaded by West Lake University on 2/18/2024 5:45:26 PM.

ions like Si can adopt very stable configurations to form layers within specific crystallographic planes in the ferroelectric o-phase, but comparatively less so in the nonpolar monoclinic one. For Si or Ge doping, the shorter Si–O and Ge–O bonding would favor the formation of a tetragonal structure which leads to four shorter or longer Hf–O bonds according to theoretical calculations.[69,70] Al, and other IIIA elements, have a large ionic radius and are generally doped as trivalent, which is conducive to the introduction of oxygen vacancies. Doped ions and oxygen vacancies play a role in both structural stabilization and induced polarization. The same is true for rare earth elements with larger radii, and the results of the experiments illustrate their advantages. Moreover, the dopant ordering is interestingly found to yield a FE ground state and the usual paraelectric phase becoming a higher-energy metastable polymorph.[71] More recently, Xue *et al.*[66] further suggest that the ionic radii and coordination number of the doped HfO_2 would have a significant impact on the origin of the ferroelectricity and the switching path that finally relates to the fatigue phenomena. The coordination number in ionic compounds is specified according to the bond angles, and anions considered as close neighbors of cations should have bond angles of not less than 65°, which is more in line with the case of various elements with different ionic sizes, and is another feasible aspect to understand to defects effect.[66]

In addition to the experimental work available, theoretical work is also being carried out extensively. Rohit *et al.*[38] studied the effect of nearly 40 dopants on the stabilization of the polar $Pca2_1$ phase by theoretical calculations. They predicted that the lanthanide series metals, the alkaline earth metals (Ca, Sr, and Ba) and Y as the most suitable dopants to promote ferroelectricity in hafnia (Fig. 8c). We summarized all the current data for the remnant polarization depending on the ionic radius for different dopants. La, Tm, and Al are favorable for inducing much higher P_r of over 40 $\mu C\ cm^{-2}$. While Al doped HfO_2 shows a coercive field ($\sim$4 MV cm^{-1})[89] about two times larger compared with that of the La doped case ($\sim$2 MV cm^{-1}).[6] Rare earth elements, such as Sc and Y, can generally be helpful to drive the HfO_2 phase transition to the o/t/c phase. Si and Ge are able to induce antiferroelectric behaviour, which has not been observed in N, Sc, and Y doped cases.

It is also worth noting that the transition from the t-phase to ferroelectric o-phase during the wake-up of Si-[92] or Zr-doped[90] HfO_2 may be accompanied by an anti-ferroelectric (AFE)-like behaviour and the appearance of double peaks in the polarization current loop, which can be suppressed by changing the doping concentration and which also occurs in similar ZrO_2 structures.[93] This is consistent with the doping induced ferroelectricity associated with an enlarged ratio of dopants.[6,47,72–89] This is significantly different from that of the conventional perovskite ferroelectrics where dopants generally can't easily induce a nonferroelectric-ferroelectric phase transition.

3.2 Zr doping in HfO_2

Zr is an element with relatively close properties to Hf, though it looks like doping Zr into the HfO_2, the doping level of Zr can be over 20% to form HfO_2–ZrO_2 solid solution, which makes it different to that of the normal mono-doping cases, with a doping level generally below 10%. Moreover, their binary oxides have similar configurations and are widely applied in HfO_2-based ferroelectrics,[90] so the Zr doping and $Hf_xZr_{1-x}O_2$ (HZO) system is described here separately. The introduction of Zr elements is of great importance in regulating the properties and saving costs, and HZO solid solution is a very important one in hafnium oxide based ferroelectric materials. As shown in Fig. 9a, ferroelectricity can be achieved in mixed HZO,[90] while Si doped HfO_2 also shows a doping-level-dependent antiferroelectric to ferroelectric transition (Fig. 9b and c).[93] Among the

 This journal is © The Royal Society of Chemistry 2024

Published on 29 November 2023. Downloaded by West Lake University on 2/18/2024 5:45:26 PM.

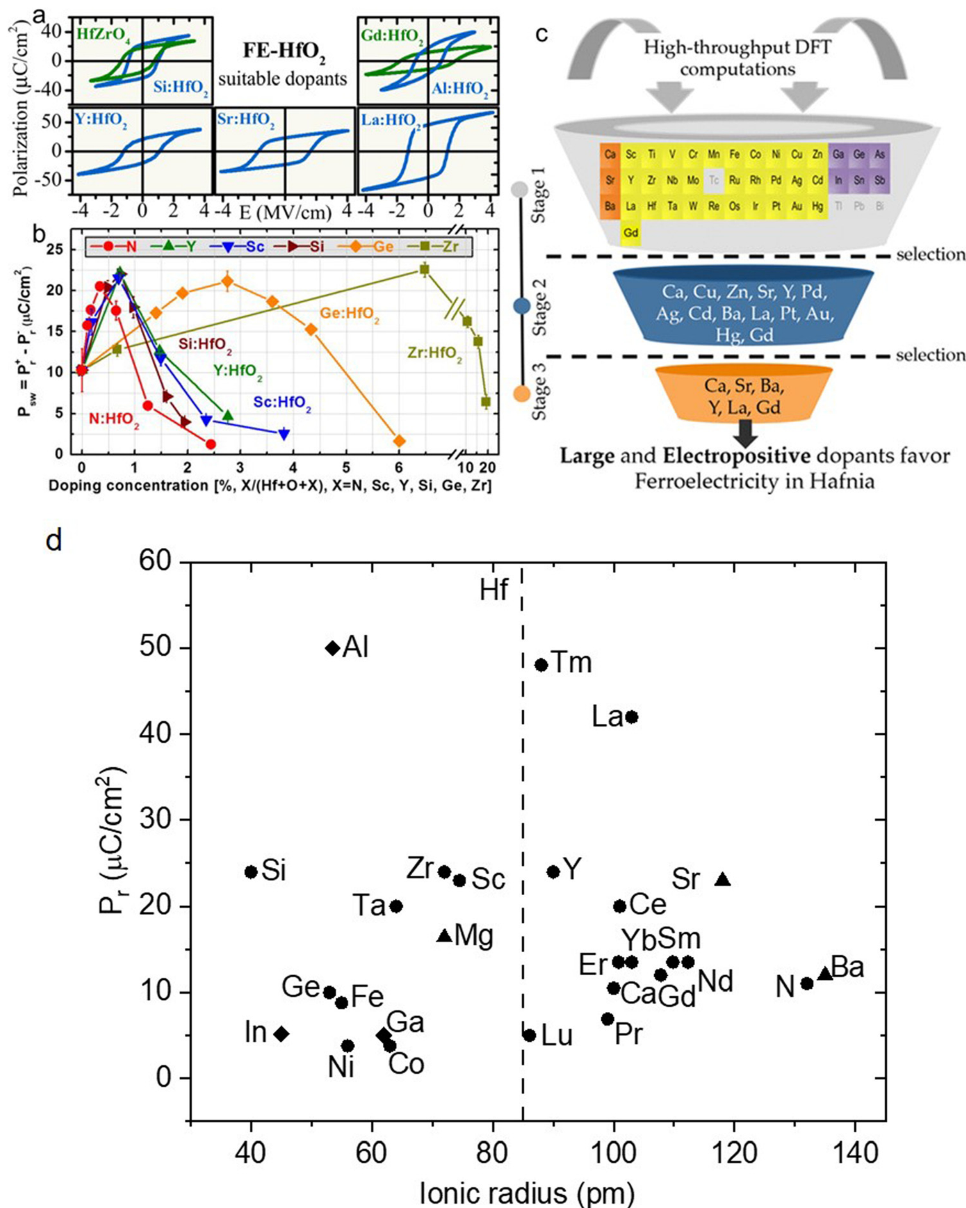

Fig. 8 (a) Hysteresis lines for TiN/8–10 nm X:HfO_2 (X = Y, Si, Gd, La, Sr, Al) or $HfZrO_4$/TiN capacitors with X in HfO_2 < 10 mol% and a maximum P_r of ∼45 μC cm^{-2} was obtained for films of La:HfO_2.[6] (b) Switchable polarization PSW of 27 (±2) nm HfO_2 films is shown as a function of doping concentrations for different dopants: Sc, Y, Si, Ge, Zr, and N.[72] (c) Three stages of dopant element selection by DFT calculation.[38] Remnant polarization depending of the ionic radius for different dopants (a six coordination number is used for all elements for the ionic radius). The data points for the rare earth metals are taken from a previous publication.[6,72–90] Ionic radius data are from the table of effective ionic radii by R. D. Shannon.[91]

proposed dopants for HfO_2, Zr has nearly identical crystal phases, lattice parameters, and atomic radius as Hf, which makes its integration into HfO_2 more feasible. The concentration window where ferroelectricity appears was reported to be much wider for the HZO system.[90] Among the HfO_2-based ferroelectrics, ferroelectric HZO is widely applied due to its large-scale preparation *via* atomic layer deposition (ALD).

3.3 Mixed ion co-doping

Both mono-ion doping and HZO solution can be helpful to stabilize the metastable ferroelectric phase and enhance the ferroelectricity. Actually, in addition to mono-ion doping, mixed ion co-doping strategies in defect-engineering, such as acceptor-donor co-doping and aliovalent ion co-doping, have been widely used to tune the dielectric behaviour of metal oxides.[94] For example, colossal permittivity behaviour in acceptor-donor co-doped TiO_2.[95,96] One of the interesting points in co-doping is that the acceptor and donor can mutually assist the diffusion into the matrix and also that the co-doping ions can form defect-dipolar clusters where the dipolar moment can be high enough to affect the ferroelectric polarization.[97]

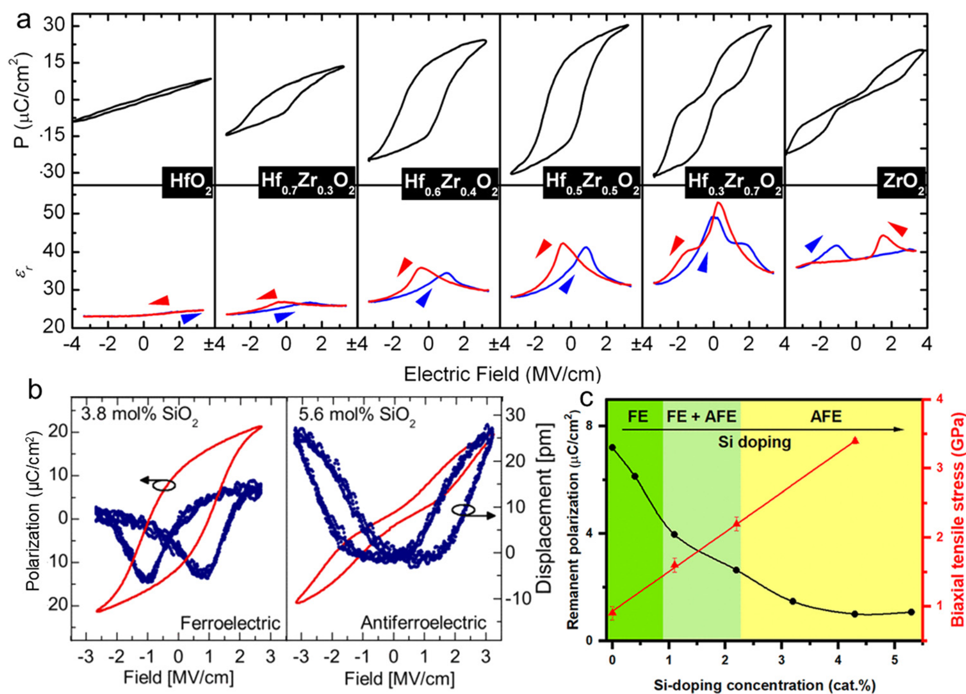

Fig. 9 (a) PV hysteresis at 1 kHz and small signal CV hysteresis at 10 kHz (50 mV level) of 9 nm thin HfO_2–ZrO_2 based metal–insulator–metal capacitors at room temperature. An evolution from paraelectric HfO_2 to ferroelectric HfO_2–ZrO_2 to an antiferroelectric-like behavior in ZrO_2 can be observed in PV as well as in CV characteristics.[90] (b) Polarization and piezoelectric displacement measurements (double beam laser interferometer) of MIM capacitor samples with ferroelectric and antiferroelectric HfSiO insulators.[92] (c) The concentration of Si doping in ZrO_2 affects the FE-AFE properties of the material.[93]

Doping two kinds of elements in the HfO_2 may simultaneously open up the possibility of engineering the local distortion and dynamic behaviour of the ferroelectric metastable phase in addition to mono-ion doping. Patrick *et al.*[99] reported Al + Si co-doped HfO_2 with remnant polarization of $\sim$20 μC cm^{-2} and enhanced endurance up to 10^8 cycles. Mihaela *et al.*[98] investigated La + Y/Gd co-doped HZO, and as shown in Fig. 10, the (Y, La) or (Gd, La) co-doped HZO thin films were found to increase the amount of o- and t- phases (Fig. 10a and b). Moreover, the cycling experiments indicate a fatigue free capacitor with remnant polarization over 15 μC cm^{-2} at 1×10^{11} endurance cycles (Fig. 10c and d). The presence of two dopants is believed to induce a larger structural distortion within HZO due to the differences in the ionic radius between both dopants. The distortion-induced strain can modulate the relative t-/o- phase content, and it is beneficial for the reduction in the number of high-symmetry phases and suppresses the monoclinic phase.

3.4 Oxygen migration and phase transitions

The above sections suggest the change in oxygen vacancy concentration is one of the origins of phase evolution. For tetravalent dopant like Si, the stabilization of high symmetric phases may originate from the distortion of the HfO_2 lattice. Meanwhile, cooperation of bivalent or trivalent dopants in the lattice will introduce a significant amount of oxygen vacancies for charge compensation, which may be the root-cause of stabilizing high symmetric phases. In addition to electric measurements, direct evidence of the thermodynamic behaviour of the metastable phase and phase transition in relation to the oxygen vacancy would be favorable to provide an in-depth understanding of the role of oxygen vacancies.

As shown in Fig. 11a–c, through direct imaging of oxygen, Nukala *et al.*[49] provided evidence of reversible and hysteretic migration of oxygen vacancy (V_O) from the bottom to the top electrode through the HZO layer. Associated with this migration, V_O induces phase transitions in the LSMO (bottom electrode) and HZO layers where the intrinsic ferroelectric switching is intertwined with extrinsic factors of oxygen voltammetry due to thermally activated oxygen migration.[11,87] Fig. 11d shows schematically how the oxygen chemical potential influences the density of defects in the lattices of ferroelectric o-HfO_2 and o-HZO. Under a pure o-phase without defects, ideally high ferroelectric polarization can be achieved due to the ordered dipole moment under an electric field. For practical polymorph HfO_2 film and its defects, the ferroelectricity would be poor in oxygen-rich conditions as a low fraction of ferroelectric O-phase in films. The low fraction of the O-phase is suggested to be caused by both oxygen-rich conditions and the negative formation energy of neutral oxygen compared with the t-phase.[11,87] Nico *et al.*[100] reported oxygen vacancy-induced phase transition from the monoclinic to rhombohedral phase (Fig. 11e). Even recently, based on the lattice-mode-matching criterion, Ma *et al.*[101] systematically studied the phase transitions between different polymorphs of hafnia under the influences of natural and positively charged oxygen

This journal is © The Royal Society of Chemistry 2024

Published on 29 November 2023. Downloaded by West Lake University on 2/18/2024 5:45:26 PM.

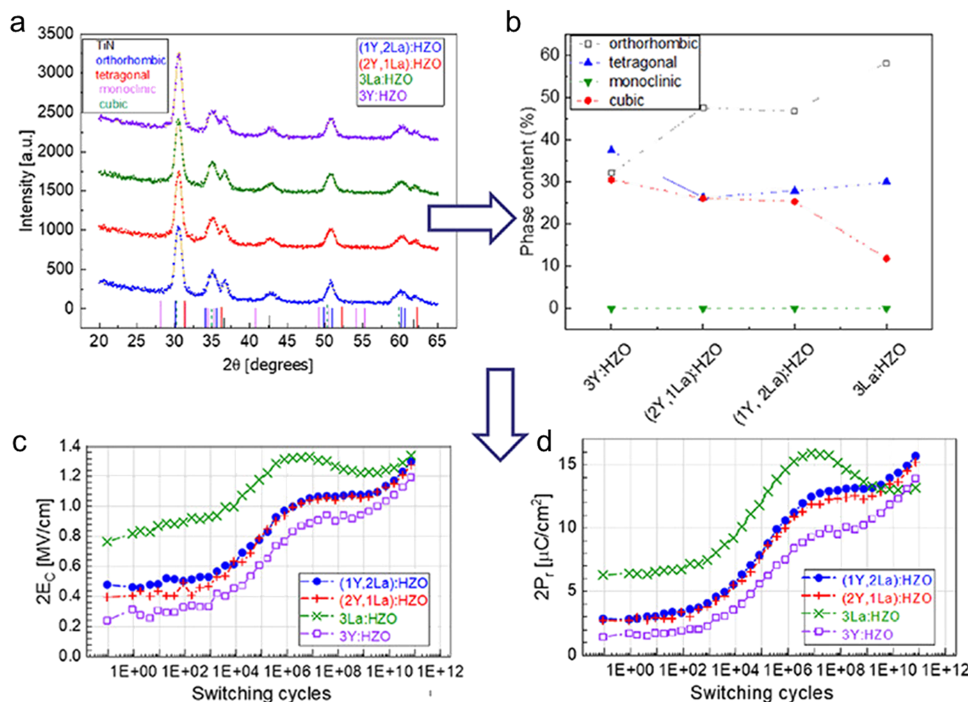

Fig. 10 Grazing incidence X-ray diffraction (GIXRD) spectra (dot) and data fit (beige line) (a) and the computed phase content of ∼12 nm Gd-doped HZO as a function of the Gd concentration (at%) and of the initial $2P_r$ (b), $2P_r$ (c) and $2E_c$ (d) as a function of switching cycles of several ∼9.5 nm HZO layers doped and/or co-doped with Y and/or La, measured at an applied electric field magnitude of 2.5 MV cm^{-1}.[98]

Published on 29 November 2023. Downloaded by West Lake University on 2/18/2024 5:45:26 PM.

vacancies using a first-principles-based variable-cell nudged elastic band method. As shown in Fig. 11f, the atomic displacements of polar oxygen atoms in polar-O phase HfO_2 are insensitive to charge-carrier doping, indicating an extremely charge-carrier inert ferroelectricity of the polar-O phase. Fig. 11g and h show the comparison of transition pathways between m (M), t (T), and polar o-phase (O) in the presence of neutral oxygen vacancies and charged oxygen vacancies, respectively. The much lower energy barrier in the latter one between the M–O phase transition suggests that the ferroelectric phase transition is kinetically favored by the charged oxygen vacancies. This demonstrates structural polymorphism kinetics promoted by the charged oxygen vacancies in HfO_2, which provide novel insight in the ferroelectricity origin and would guide further property optimization in the HfO_2-based system.

3.5 Interface-engineered dynamic behaviour of oxygen vacancy

The above discussion about point defects is generally an intragrain behaviour where the oxygen vacancies can be compositionally modulated by the doping of aliovalent dopants. The oxygen vacancy migration is suggested to be thermodynamically related to the phase transition in the thin films under an external electric field. In addition to the compositional modulation, interface-engineering is suggested to be another promising way to modulate the thermodynamic behaviour of the oxygen vacancies.

Recently, Popovici *et al.*[103] reported high-performance La-doped HZO based ferroelectric capacitors *via* a cap layer. By incorporating either a 1 nm TiO_2 and/or 2 nm Nb_2O_5 cap layer in a bilayer (BL) or trilayer configuration as shown in Fig. 12a. Obvious diffraction peaks indexed with the o-phase can be observed in the GIXRD pattern, and the increased content of orthorhombic phase was further confirmed from precession electron microscopy. The insertion of the TiO_2 and Nb_2O_5 interface can obviously enhance the ferroelectricity with higher P_r and reduced wake-up. Endurance of up to 10^{11} cycles with a final P_r of ∼15 μC cm^{-2} at 1.8 MV cm^{-1} can be obtained. The interface layer Nb_2O_5 is suggested to act as a V_O sink when in contact with HZO, which can facilitate the desired t-phase to o-phase transition, while the TiO_2 is used to enhance the amount of grains in the preferred o(002) grain orientation. Zhang *et al.*[104] demonstrated that the wake-up and fatigue phenomena are strongly affected by the interfacial layer-controlled depolarization field that can increase the thickness of the interfacial layer during electric cycling. The interface layer is suggested to manipulate the electrical properties of the HZO devices based on the types of electrode match and hybrid cycling process.

From the above results, it can be determined that the dopant-induced ferroelectric phase transition is a general phenomenon at a critical doping level in doped HfO_2. A higher doping level is more likely to stabilize the non-ferroelectric phase. However, among the point defects, oxygen vacancy is vital for the phase transition and stabilization, especially in trivalent rare-earth element doped HfO_2 where generally high remnant polarization can be achieved. Moreover, the interface modulated ferroelectricity is rather effective to enhance ferroelectricity and endurance.

Published on 29 November 2023. Downloaded by West Lake University on 2/18/2024 5:45:26 PM.

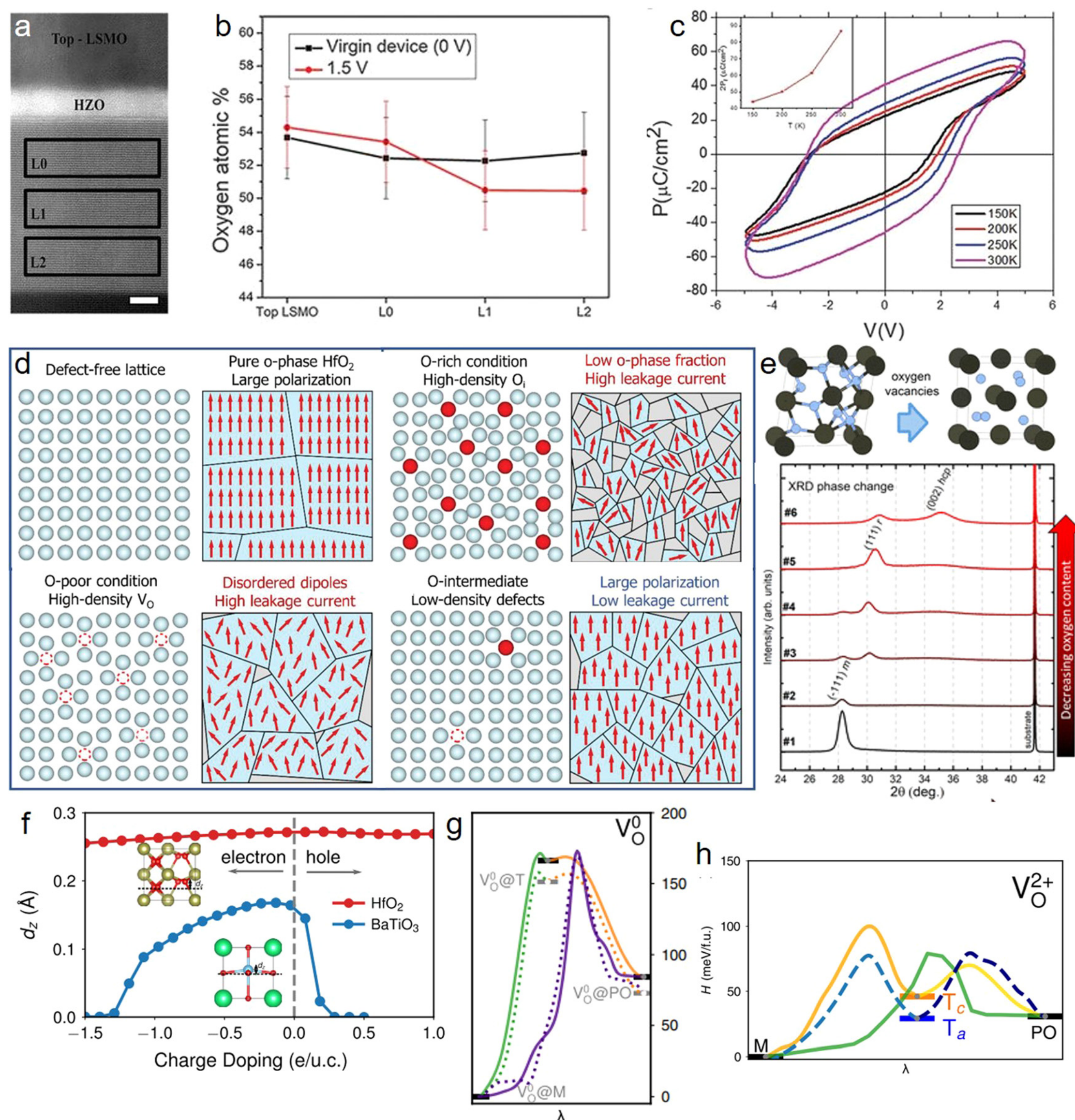

Fig. 11 Overview image of the LSMO/HZO/LSMO capacitor (a) with regions marked where the oxygen content was quantified from EDS (b) at 0 V and 1.5 V. (c) Temperature-dependent *P*–*V* loops obtained from dynamic hysteresis measurements at 1 kHz in LSMO/HZO (7 nm)/LSMO (30 nm) capacitors.[11] (d) Oxygen content-dependent structural transformation from monoclinic m-HfO_2 to rhombohedral hafnium oxide (r-$HfO_{1.7}$) and sketches of the calculated structures corresponding to m-HfO_2 and r-$HfO_{1.5}$.[100] (e) A schematic plot of how the O chemical potential influences the density of defects in the lattices of ferroelectric orthorhombic HfO_2 and (Hf, Zr)O_2.[102] (f) Polar atomic displacement (d_z) as a function of charge-carrier concentration for the polar o-phase of HfO_2 and tetragonal $BaTiO_3$. The inset image shows the definition of d_z in HfO_2 and $BaTiO_3$. (g) Minimum energy pathways connecting different polymorphs of HfO_2 obtained with VCNEB. (h) Comparison of transition pathways between M, T, and polar-O (PO) phases at the pristine state (solid lines) and those in the presence of V_O at a concentration of 3.125% (dashed lines). The energy of the M phase is chosen as the energy zero point.[101]

3.6 Defect-induced flattening of the polar phonon band

Though defects are widely introduced to improve the emergent ferroelectricity by its kinetic promotion effect in the phase transition (Fig. 13a), their roles are still not fully understood at the atomic level especially when considering the correlation between point defects and lattice.

In recent studies, we have calculated the lattice vibrational states corresponding to flat polar phonon modes in La doped fluorite MO_2 (M = Hf, Zr) to understand the reason at an atomic level (Fig. 13b–i).[8] It is found that both La doped and V_O-only doped MO_2 show significantly flattened polar phonon bands. Different from the localized electric dipoles with sharp zero-width domain walls in pure O-MO_2, the point-defect-induced local symmetry breaking in doped cases lead to a collective electric polarization across the point-defect, which somehow diffuses the domain walls. However, Fig. 13j shows that although La-doping can enhance the remnant polarization, the coercive field will also become larger. In contrast, only moderate V_O-doped cases can induce both enhanced remnant

Published on 29 November 2023. Downloaded by West Lake University on 2/18/2024 5:45:26 PM.

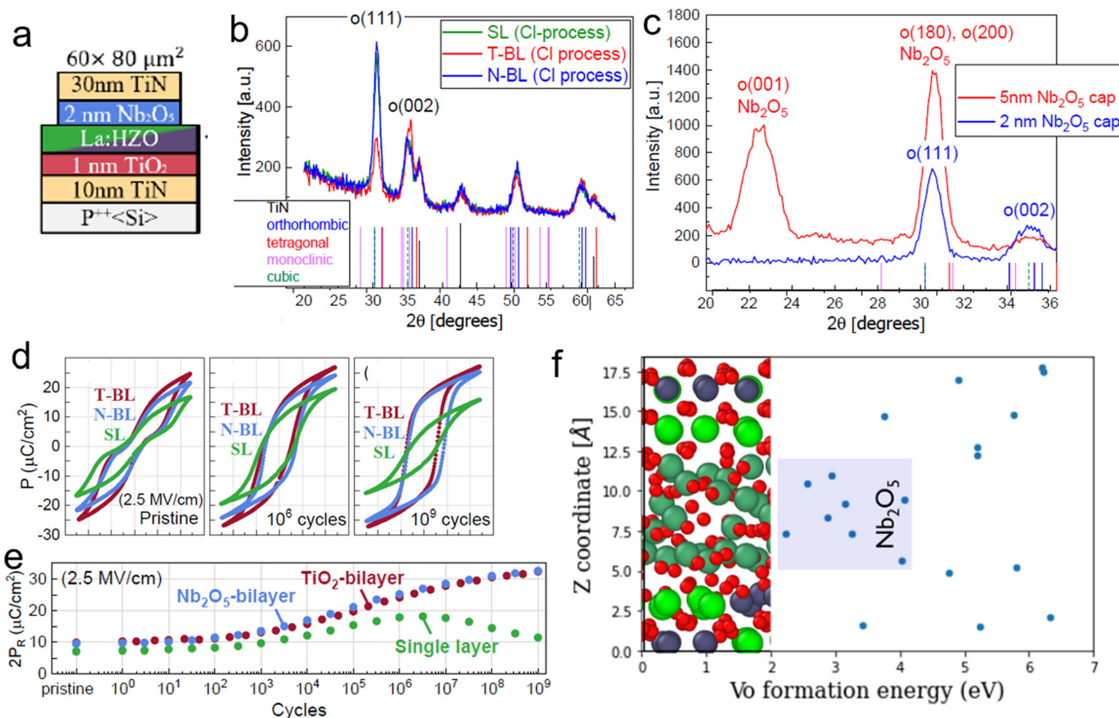

Fig. 12 Schematic illustration of the heterostructure, GIXRD patterns of the single layer (SL, green) (b), and a N–BL stack with 2 nm (blue) or 5 nm (red) Nb_2O_5 (c) are plotted together with the reference diffraction peaks for the m-, o-, t-, and c-phase of ZrO_2 and cubic TiN. All the stacks were derived from the CL-process. (d) Polarization hysteresis of the single layer (SL, green), TiO_2-bilayer (T–BL, red) and Nb_2O_5-bilayer (N–BL, blue) in the case of the pristine device, and after 10^6 cycles and 10^9 cycles. (e) $2P_r$ *vs.* switching cycles for the single layer (SL, green), TiO_2-bilayer (T–BL, red) and the Nb_2O_5-bilayer (N–BL, blue). All the measurements have been performed at 2.5 MV cm^{-1}. (f) Density functional theory computed V_O formation energies in the HZO/Nb_2O_5 stack show a greater affinity for oxygen vacancies (lower formation energies) in the Nb_2O_5 (*z*-coordinate between 5 and 12.5 A), which plays the role of Vo sink in contact with HZO, in the inset •-O, •-Zr, •-Hf and •-Nb.[103]

polarization and a lower barrier energy, which suggest that V_O and local lattice distortion should be balanced for high-performance fluorite ferroelectricity.

4 Thin film preparation and ion-bombardment doping

Film preparation methods could have an impact on film properties, with effects coming from factors such as temperature, humidity, and vacuum. A variety of techniques and methods have been invented for the preparation of ferroelectric film. Ferroelectric HfO_2 films with high P_r values have been fabricated by pulsed laser deposition (PLD),[31] ALD,[109] sputtering deposition,[110,111] and chemical solution deposition (CSD).[85,112]

Each of these methods have their advantages and disadvantages, and the most intensively used deposition method is ALD due to its ultra-thin growth, low-temperature deposition, and semiconductor process compatibility, *etc.*[113] ALD can generally control the $Zr_xHf_{1-x}O_2$ by controlling the number of Zr layers in the HfO_2-based system. Therefore, ALD is limited in its ability to achieve homogenous and low-level doping. Upon ALD, surface treatment by using ozone (O_3) or ion bombardment has been used to engineer the surface state and defects in the thin films.

Recently, in addition to aliovalent doping and solid solution, the control of ALD O_3 dose,[114] oxygen content in sputtering methods,[115] and control of nitrogen flow in electrode deposition,[116] have also been reported to induce ferroelectricity. For example, Fig. 14a and b show the ferroelectric polarization of HfO_2 under different annealing temperatures and O_3 doping time, where in both cases ferroelectricity is reduced. Similar reduced ferroelectricity and even higher leaky current were observed in oxygen vacancy doped HfO_2 (Fig. 14c–e). Hu *et al.*[117] reported nitrogen-oxyanion-doped HfO_2 to have an enhanced on/off ratio and endurance. More research is needed on the nature of ferroelectric formation in conjunction with oxygen-tuning during the preparation method.

However, the appearance of ion bombardment that has been conventionally used in doping semiconductor, has drawn increasing attention in treating other material systems. Compared with surface treatment with O_3 or nitrogen flow, ion bombardment is going to be a game changer due to its flexibility in treating the surface and doping the materials depending on the energy and type of the ion source.[120] Kang *et al.*[121] found that the ferroelectric properties improve by bombarding films of hafnium oxide with a beam of helium ions. As shown in Fig. 15a and b, the ion bombardment creates oxygen vacancies and strain changes from helium implantation that pushes more of the polycrystalline samples into the

Published on 29 November 2023. Downloaded by West Lake University on 2/18/2024 5:45:26 PM.

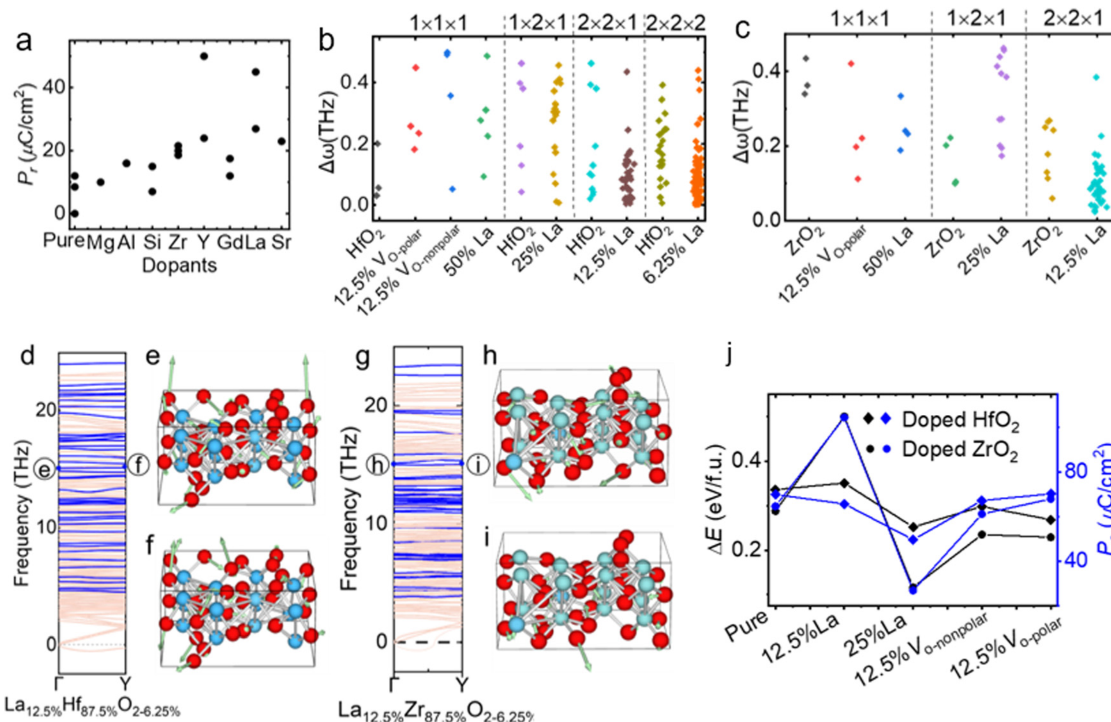

Fig. 13 Point-defect-induced flattening of phonon band structures in La-doped fluorite MO_2 (M = Hf, Zr). (a) Mapping of reported typical maximum remnant polarization values in pure and doped fluorite-based metal oxides MO_2 (M = Zr, and Hf) with different dopants.[17,47,83,84,90,92,105–108] (b) and (c) Comparison of the absolute values of the frequencies ($\Delta\omega < 0.5$ THz) of the polar bands from Γ to Y wave vectors for pristine and the doped cases with the same size supercells. (d) Phonon spectra of $La_{12.5\%}Hf_{87.5\%}O_{2-6.25\%}$ where the flat polar phonon modes from Γ (~15.08 THz) and Y (~15.10 THz) wave vectors are indicated in (e) and (f), respectively. (g) Phonon spectra of $La_{12.5\%}Zr_{87.5\%}O_{2-6.25\%}$ where the flat polar phonon modes from Γ (at 15.02 THz) and Y (at 15.05 THz) wave vectors at ~15.1 THz were indicated by (h) and (i), respectively. Vo-nonpolar and Vo-polar mean the site of V_O in the nonpolar region (spacer layer) and polar region (ferroelectric layer), respectively. (j) Evolution of energy barrier ΔE and spontaneous polarization (P_S) values in doped MO_2 (M = Hf, Zr).[8]

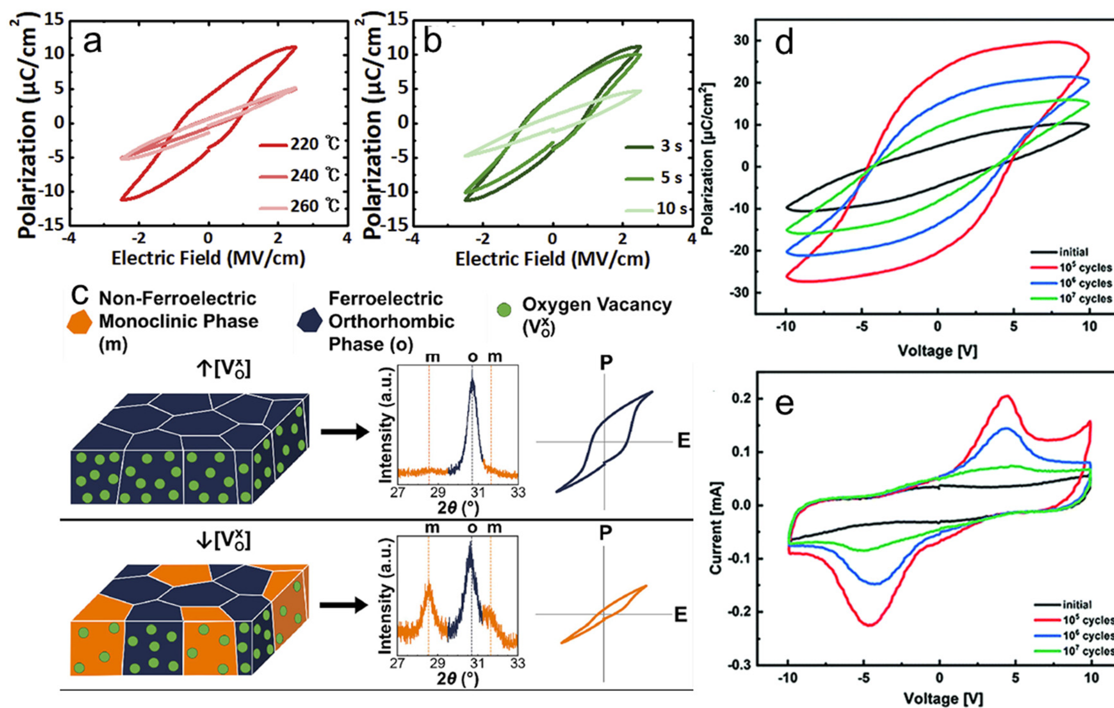

Fig. 14 Variations in P–E curves for the MFM capacitors using HfO_2 thin films prepared (a) at different ALD temperatures and (b) with different O_3 dose times.[118] (c) Effect of oxygen content on the phase composition and ferroelectricity of magnetron sputtered films.[110] (d) and (e) P–V, I–V curves of 136 nm films prepared by CSD.[119]

 This journal is © The Royal Society of Chemistry 2024

View Article Online

Published on 29 November 2023. Downloaded by West Lake University on 2/18/2024 5:45:26 PM.

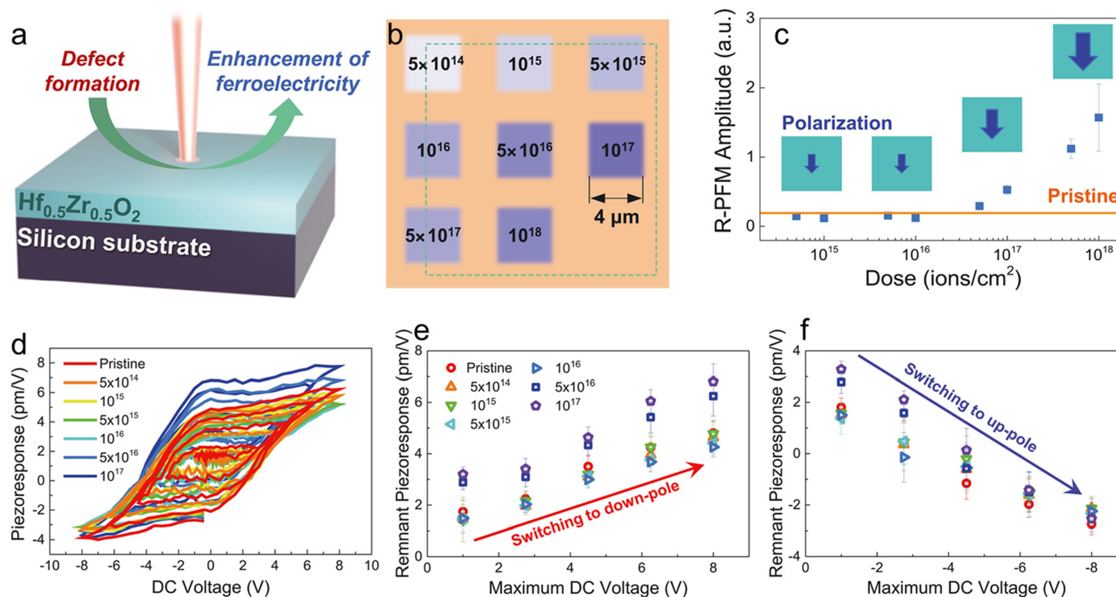

Fig. 15 (a) Schematic representation of the ion bombardment process. (b) Scheme for the dose of He ion bombardment; inserted texts indicate the He ion doses (ions per cm^2). (c) R-PFM amplitudes as a function of He ion dose. (d) FORC-PFM hysteresis loop depending on the He ion dose. (e) Positive and (f) negative remnant piezoresponse *versus* $V_{dc,max}$ depending on the He ion dose.[121]

ferroelectric orthorhombic phase.[121] Helium ion bombardment following ALD preparation of thin films has emerged as a new strategy to explore ferroelectricity. They deposited 10 nm thick HZO films by ALD and PLD, respectively, and demonstrated the high enhancement of ferroelectricity in HZO films based on He ion bombardment dose according to piezoresponse force microscopic analysis (Fig. 15d–f). It is suggested that the large enhancement of ferroelectricity by ion bombardment might be caused by the uniform distribution of oxygen vacancies and the phase transition to the ferroelectric phase. Similarly in conventional ferroelectrics, Chen *et al.*[122] used helium ion implantation to induce an ordered-disordered (antiferroelectric–relaxed ferroelectric-like) phase transition in antiferroelectric PZO epitaxial films to obtain ferroelectric domains at the nanoscale, demonstrating that the introduction of highly disordered microstructural features by ion implantation is an effective post-processing method for flexible modulation of material structures and physical properties. One should note that bombardment with different ions, not just He, can be used to achieve doping as well as modulation of oxygen vacancies.[120] In this consideration, ion bombardment would be promising to flexibly achieve doping in HfO_2-based ferroelectrics.

This method may become an important tool for stabilizing the ferroelectric phase for the next generation of electronic devices. Theoretical calculations of the thermodynamic mechanism allow us to explore possible mechanisms for ion bombardment-enhanced polarization. Moreover, one should note that bombardment ions are not limited to He, ions like Si and Al can also be selected, depending on the radiation source used.[120] Even radiation with a high electron beam would also be a promising way to modulate the properties of HfO_2-based ferroelectrics.[123] Based on the advances in the ion bombardment techniques, ultimately, this approach can be directly applied to semiconductor processes without structural modifications, thus increasing its applicability in next-generation electronic devices, such as super-scale ferroelectric-based transistors and memories.

5 Summary and prospect

Summary

In this review we discussed the ferroelectricity origin of HfO_2, the influence of defects on the formation of ferroelectric phases and the methods of preparation. The ferroelectricity has been reported to originate from the polar orthorhombic phase $Pca2_1$ and the polar rhombohedral phase $R3m$ or $R3$, transformed from either the t-phase or the m-phase. Moreover, the different pathways of the polarization switching mechanism are reviewed in $Pca2_1$, and the uncertain mechanism in $R3m$ is proposed for more exploration. Doping, oxygen vacancies, and the interface effect are important considerations in the formation of the ferroelectric sub-stable phase in HfO_2-based thin films, which is different from the ferroelectricity origin in conventional ferroelectrics. In numerous studies, appropriate doping can generally enhance the ferroelectric remnant polarization. Furthermore, the phase transition of the HfO_2-based system is kinetically related to the migration of intrinsic defects of oxygen vacancies, which is also responsible for the more flattened phonon band and making the domain walls become slightly diffused. A sophisticated interfacial capping layer can act as a V_O sink to enhance the endurance of polarization by facilitating the migration in phase transition.[11] ALD together with ion bombardment are promising for doping engineering in a HfO_2-based system for large scale electronic device fabrication. However, though the ferroelectricity can be somehow

Published on 29 November 2023. Downloaded by West Lake University on 2/18/2024 5:45:26 PM.

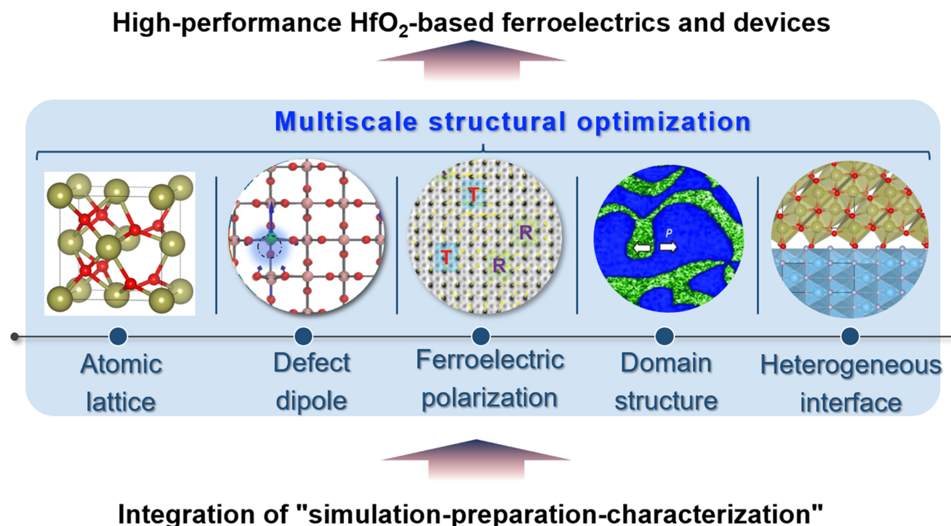

Fig. 16 Schematic illustration of the multiscale structure optimization for high-performance HfO_2-based ferroelectrics and devices based on integration of "simulation–preparation–characterization".

improved by doping engineering, ferroelectric devices with high stability, high endurance and high remnant polarization are still challenging to realize.

Outlooks

As discussed above, impurity ions, oxygen vacancies, and interface are three important factors affecting the properties of HfO_2-based ferroelectrics. Considering that doping can improve remnant polarization and endurance, a combination method of the above factors would provide a promising way to comprehensively optimize their ferroelectric performance. Therefore, as shown in Fig. 16, we believe that further optimization of the HfO_2-based ferroelectrics and devices should consider a collaboration of multilevel-structure polarization components and even machine learning,[124] including lattice vibration, defect-dipoles, ferroelectric polarization, domain structures, and heterogeneous interface.

In this consideration, an integration of "simulation–preparation–characterization" would be favorable to comprehensively clarify the micro mechanism and optimize the ferroelectric performance of the HfO_2-based system. The polarization switching mechanism and phonon band under the defect effect would be an interesting approach to understand the novel properties in HfO_2-based ferroelectrics. A combination of theoretical density functional theory calculations, molecular dynamic simulations and phase field modeling, would provide a promising multi-scale approach to cover all the important factors to design and optimize the ferroelectricity of the HfO_2-based system. This part is still lacking and requires more research endeavors to be established.

Currently, most ion doping in ALD-prepared HfO_2 relies on layer-doping due to the growth nature of the ALD process. In considering this, ion bombardment would be another ideal way to carry out defect-engineering in ALD-prepared HfO_2-based ferroelectrics at a low doping level. The interface layer would be more precisely considered the one with large V_O-migration flexibility in order to provide a V_O sink. Therefore, a V_O ionic conductor would be a promising candidate and requires further work to be established.

Author contributions

WD initiated the project. FY wrote the manuscript with the assistance from YW, PA, KX, SL, SD, and YL. WD and QF analyzed the data with the assistance from XH, LY, GZ, WL, and SJ. PA, FY and WD wrote the manuscript. All the authors revised and polished the manuscript.

Conflicts of interest

The authors declare no competing interests.

Acknowledgements

W. D. acknowledges the National Key Research and Development Plan (2021YFA1202100), the Nature Science Foundation of Hubei province (20223564/2022CFB595) and China (52202134), the 2021 Independent Innovation Fund-New Teacher Research Starting Fund of Huazhong University of Science and Technology (5003182109) and the Innovation Fund of WNLO, 2022 Shenzhen Central Leading Local Science and Technology Development Special Funding Program Virtual University Park Laboratory Project. Q. F. acknowledges the Natural Science Foundation of China (61971459), and the Shenzhen Technology Plan (JCYJ20190809095009521).

References

1 T. Mikolajick, S. Slesazeck, M. H. Park and U. Schroeder, *MRS Bull.*, 2018, **43**, 340–346.
2 M. Kumar and H. Seo, *Adv. Mater.*, 2022, **34**, 10.

 This journal is © The Royal Society of Chemistry 2024

Published on 29 November 2023. Downloaded by West Lake University on 2/18/2024 5:45:26 PM.

3 C. Mart, A. Viegas, S. Esslinger, M. Czernohorsky, W. Weinreich, D. Mutschall, A. Kaiser, N. Neumann, T. Grossmann, K. Hiller and L. M. Eng, *Ieee, Electr Network*, 2020.

4 A. Fernandez, M. Acharya, H.-G. Lee, J. Schimpf, Y. Jiang, D. Lou, Z. Tian and L. W. Martin, *Adv. Mater.*, 2022, **34**, 2108841.

5 J. F. Scott and C. A. Paz de Araujo, *Science*, 1989, **246**, 1400–1405.

6 J. Müller, T. S. Böscke, S. Müller, E. Yurchuk, P. Polakowski, J. Paul, D. Martin, T. Schenk, K. Khullar, A. Kersch, W. Weinreich, S. Riedel, K. Seidel, A. Kumar, T. M. Arruda, S. V. Kalinin, T. Schlösser, R. Boschke, R. V. Bentum, U. Schröder and T. Mikolajick, *IEEE Int. Electron Devices Meet.*, 2013, 10.18.11–10.18.14.

7 H. J. Lee, M. Lee, K. Lee, J. Jo, H. Yang, Y. Kim, S. C. Chae, U. Waghmare and J. H. Lee, *Science*, 2020, **369**, 1343–1347.

8 P. Ai, F. Yan, W. Dong, S. Liu, J. Zhao, K.-H. Xue, S. U. H. Bakhtiar, Y. Liu, Q. Ma, L. Miao, M. Hua, G. Zhang, S. Jiang, W. Luo and Q. Fu, *npj Comput. Mater.*, 2023, **9**, 119.

9 X. H. Xu, F. T. Huang, Y. B. Qi, S. Singh, K. M. Rabe, D. Obeysekera, J. J. Yang, M. W. Chu and S. W. Cheong, *Nat. Mater.*, 2021, **20**, 826–832.

10 H. Lee, D.-H. Choe, S. Jo, J.-H. Kim, H. H. Lee, H.-J. Shin, Y. Park, S. Kang, Y. Cho, S. Park, T. Moon, D. Eom, M. Leem, Y. Kim, J. Heo, E. Lee and H. Kim, *ACS Appl. Mater. Interfaces*, 2021, **13**, 36499–36506.

11 P. Nukala, M. Ahmadi, Y. Wei, S. de Graaf, E. Stylianidis, T. Chakrabortty, S. Matzen, H. W. Zandbergen, A. Björling, D. Mannix, D. Carbone, B. Kooi and B. Noheda, *Science*, 2021, **372**, 630–635.

12 T. S. Böscke, J. Müller, D. Bräuhaus, U. Schröder and U. Böttger, *Appl. Phys. Lett.*, 2011, **99**, 102903.

13 Q. Luo, Y. Cheng, J. Yang, R. Cao, H. Ma, Y. Yang, R. Huang, W. Wei, Y. Zheng, T. Gong, J. Yu, X. Xu, P. Yuan, X. Li, L. Tai, H. Yu, D. Shang, Q. Liu, B. Yu, Q. Ren, H. Lv and M. Liu, *Nat. Commun.*, 2020, **11**, 1391.

14 B. Ku, S. Choi, Y. Song and C. Choi, *2020 IEEE Symposium on VLSI Technology*, 2020, 1–2.

15 X. Liu, L. Yao, Y. Cheng, B. Xiao, M. Liu and W. Wang, *Appl. Phys. Lett.*, 2019, **115**, 152901.

16 K.-W. Huang, S.-H. Yi, Y.-S. Jiang, W.-C. Kao, Y.-T. Yin, D. Beck, V. Korolkov, R. Proksch, J. Shieh and M.-J. Chen, *Acta Mater.*, 2021, **205**, 116536.

17 Y. Yun, P. Buragohain, M. Li, Z. Ahmadi, Y. Zhang, X. Li, H. Wang, J. Li, P. Lu, L. Tao, H. Wang, J. E. Shield, E. Y. Tsymbal, A. Gruverman and X. Xu, *Nat. Mater.*, 2022, **21**, 903–909.

18 L. Liu and H. Huang, *Chem. – Eur. J.*, 2022, **28**, e202103975.

19 J. Wang, H. P. Li and R. Stevens, *J. Mater. Sci.*, 1992, **27**, 5397–5430.

20 M. H. Park, Y. H. Lee, H. J. Kim, Y. J. Kim, T. Moon, K. D. Kim, J. Müller, A. Kersch, U. Schroeder, T. Mikolajick and C. S. Hwang, *Adv. Mater.*, 2015, **27**, 1811–1831.

21 P. Buragohain, C. Richter, T. Schenk, H. Lu, T. Mikolajick, U. Schroeder and A. Gruverman, *Appl. Phys. Lett.*, 2018, **112**, 222901.

22 P. Jiang, Q. Luo, X. Xu, T. Gong, P. Yuan, Y. Wang, Z. Gao, W. Wei, L. Tai and H. Lv, *Adv. Electron. Mater.*, 2021, **7**, 2000728.

23 R. Materlik, C. Künneth and A. Kersch, *J. Appl. Phys.*, 2015, 117.

24 M. Zheng, Z. Yin, Y. Cheng, X. Zhang, J. Wu and J. Qi, *Appl. Phys. Lett.*, 2021, 119.

25 A. Kersch and M. Falkowski, *Phys. Status Solidi RRL*, 2021, **15**, 2100074.

26 X. H. Sang, E. D. Grimley, T. Schenk, U. Schroeder and J. M. LeBeau, *Appl. Phys. Lett.*, 2015, **106**, 4.

27 T. D. Huan, V. Sharma, G. A. Rossetti and R. Ramprasad, *Phys. Rev. B: Condens. Matter Mater. Phys.*, 2014, **90**, 064111.

28 S. Shibayama, T. Nishimura, S. Migita and A. Toriumi, *J. Appl. Phys.*, 2018, **124**, 184101.

29 M. Falkowski and A. Kersch, *Appl. Phys. Lett.*, 2021, 118.

30 Y. Zhang, Q. Yang, L. Tao, E. Y. Tsymbal and V. Alexandrov, *Phys. Rev. Appl.*, 2020, **14**, 014068.

31 Y. Wei, P. Nukala, M. Salverda, S. Matzen, H. J. Zhao, J. Momand, A. S. Everhardt, G. Agnus, G. R. Blake, P. Lecoeur, B. J. Kooi, J. Íñiguez, B. Dkhil and B. Noheda, *Nat. Mater.*, 2018, **17**, 1095–1100.

32 Y. Wang, L. Tao, R. Guzman, Q. Luo, W. Zhou, Y. Yang, Y. Wei, Y. Liu, P. Jiang, Y. Chen, S. Lv, Y. Ding, W. Wei, T. Gong, Y. Wang, Q. Liu, S. Du and M. Liu, *Science*, 2023, **381**, 558–563.

33 Y. Cheng, Z. Gao, K. H. Ye, H. W. Park, Y. Zheng, Y. Zheng, J. Gao, M. H. Park, J.-H. Choi, K.-H. Xue, C. S. Hwang and H. Lyu, *Nat. Commun.*, 2022, **13**, 645.

34 S. S. Cheema, D. Kwon, N. Shanker, R. dos Reis, S.-L. Hsu, J. Xiao, H. Zhang, R. Wagner, A. Datar, M. R. McCarter, C. R. Serrao, A. K. Yadav, G. Karbasian, C.-H. Hsu, A. J. Tan, L.-C. Wang, V. Thakare, X. Zhang, A. Mehta, E. Karapetrova, R. V. Chopdekar, P. Shafer, E. Arenholz, C. Hu, R. Proksch, R. Ramesh, J. Ciston and S. Salahuddin, *Nature*, 2020, **580**, 478–482.

35 B. Johnson, C. M. Fancher, D. Hou and J. L. Jones, *J. Appl. Phys.*, 2019, **126**, 7.

36 T. Shiraishi, S. Choi, T. Kiguchi, T. Shimizu, H. Funakubo and T. J. Konno, *Appl. Phys. Lett.*, 2019, **114**, 232902.

37 M. H. Park, T. Schenk, C. Fancher, E. Grimley, C. Zhou, C. Richter, J. LeBeau, J. Jones, T. Mikolajick and U. Schroeder, *J. Mater. Chem. C*, 2017, **5**, 4677–4690.

38 R. Batra, T. D. Huan, G. A. Rossetti and R. Ramprasad, *Chem. Mater.*, 2017, **29**, 9102–9109.

39 F. Bohra, B. Jiang and J.-M. Zuo, *Appl. Phys. Lett.*, 2007, **90**, 161917.

40 P. D. Lomenzo, Q. Takmeel, C. M. Fancher, C. Zhou, N. G. Rudawski, S. Moghaddam, J. L. Jones and T. Nishida, *IEEE Electron Device Lett.*, 2015, **36**, 766–768.

41 Y.-C. Chiu, C.-H. Cheng, C.-Y. Chang, Y.-T. Tang and M.-C. Chen, *Phys. Status Solidi RRL*, 2017, **11**, 1600368.

Published on 29 November 2023. Downloaded by West Lake University on 2/18/2024 5:45:26 PM.

42 S. Liu and B. M. Hanrahan, *Phys. Rev. Mater.*, 2019, **3**, 054404.
43 R. Materlik, C. Kunneth, M. Falkowski, T. Mikolajick and A. Kersch, *J. Appl. Phys.*, 2018, **123**, 164101.
44 Y. Zhou, Y. K. Zhang, Q. Yang, J. Jiang, P. Fan, M. Liao and Y. C. Zhou, *Comput. Mater. Sci.*, 2019, **167**, 143–150.
45 T. Li, J. Dong, N. Zhang, Z. Wen, Z. Sun, Y. Hai, K. Wang, H. Liu, N. Tamura, S. Mi, S. Cheng, C. Ma, Y. He, L. Li, S. Ke, H. Huang and Y. Cao, *Acta Mater.*, 2021, **207**, 116696.
46 S. Mueller, J. Mueller, A. Singh, S. Riedel, J. Sundqvist, U. Schroeder and T. Mikolajick, *Adv. Funct. Mater.*, 2012, **22**, 2412–2417.
47 S. Mueller, C. Adelmann, A. Singh, S. Van Elshocht, U. Schroeder and T. Mikolajick, *ECS J. Solid State Sci. Technol.*, 2012, **1**, N123.
48 T. Schenk, C. M. Fancher, M. H. Park, C. Richter, C. Künneth, A. Kersch, J. L. Jones, T. Mikolajick and U. Schroeder, *Adv. Electron. Mater.*, 2019, **5**, 1900303.
49 Y. Tian, Y. Zhou, M. Zhao, Y. Ouyang and X. Tao, *Appl. Phys. Lett.*, 2023, **123**, 132901.
50 U. Schroeder, M. H. Park, T. Mikolajick and C. S. Hwang, *Nat. Rev. Mater.*, 2022, **7**, 653–669.
51 A. Chouprik, D. Negrov, E. Y. Tsymbal and A. Zenkevich, *Nanoscale*, 2021, **13**, 11635–11678.
52 W. Banerjee, A. Kashir and S. Kamba, *Small*, 2022, **18**, 2107575.
53 E. H. Kisi, C. J. Howard and R. J. Hill, *J. Am. Ceram. Soc.*, 1989, **72**, 1757–1760.
54 R. Batra, T. D. Huan, J. L. Jones, G. Rossetti and R. Ramprasad, *J. Phys. Chem. C*, 2017, **121**, 4139–4145.
55 W. Ding, Y. Zhang, L. Tao, Q. Yang and Y. Zhou, *Acta Mater.*, 2020, **196**, 556–564.
56 S.-T. Fan, Y.-W. Chen and C. W. Liu, *J. Phys. D: Appl. Phys.*, 2020, **53**, 23LT01.
57 H. Hasegawa, *J. Mater. Sci. Lett.*, 1983, **2**, 91–93.
58 P. Nukala, J. Antoja-Lleonart, Y. Wei, L. Yedra, B. Dkhil and B. Noheda, *ACS Appl. Electron. Mater.*, 2019, **1**, 2585–2593.
59 T. P. Smirnova, A. A. Saraev, I. V. Korolkov, V. N. Kitchai and V. O. Borisov, *J. Cryst. Growth*, 2019, **523**, 125156.
60 S. Barabash, D. Pramanik, Y. Zhai, B. Magyari-Kope and Y. Nishi, *ECS Trans.*, 2017, **75**, 107–121.
61 T. Maeda, B. Magyari-Kope and Y. Nishi, *Monterey*, CA, USA, 2017, 1–4.
62 Y.-W. Chen, S.-T. Fan and C.-Y. Liu, *J. Phys. D: Appl. Phys.*, 2020, **54**, 085304.
63 S. S. Behara and A. Van der Ven, *Phys. Rev. Mater.*, 2022, **6**, 054403.
64 Y. Wu, Y. K. Zhang, J. Jiang, L. M. Jiang, M. H. Tang, Y. C. Zhou, E. Y. Tsymbal, M. Liao and Q. Yang, *Phys. Rev. Lett.*, 2013, **131**, 226802.
65 G. Henkelman and H. Jónsson, *J. Chem. Phys.*, 2000, **113**, 9978–9985.
66 J.-H. Yuan, G.-Q. Mao, K.-H. Xue, N. Bai, C. Wang, Y. Cheng, H. Lyu, H. Sun, X. Wang and X. Miao, *Chem. Mater.*, 2023, **35**, 94–103.
67 A. Silva, I. Fina, F. Sánchez, J. P. B. Silva, L. Marques and V. Lenzi, *Mater. Today Phys.*, 2023, **34**, 101064.
68 D. Sheppard, P. Xiao, W. Chemelewski, D. D. Johnson and G. Henkelman, *J. Chem. Phys.*, 2012, **136**, 074103.
69 C.-K. Lee, E. Cho, H.-S. Lee, C. S. Hwang and S. Han, *Phys. Rev. B: Condens. Matter Mater. Phys.*, 2008, **78**, 012102.
70 D. Fischer and A. Kersch, *J. Appl. Phys.*, 2008, **104**, 084104.
71 S. Dutta, H. Aramberri, T. Schenk and J. Íñiguez, *Phys. Status Solidi RRL*, 2020, **14**, 2000047.
72 L. Xu, T. Nishimura, S. Shibayama, T. Yajima, S. Migita and A. Toriumi, *J. Appl. Phys.*, 2017, **122**, 124104.
73 C.-Q. Luo, C.-Y. Kang, Y.-L. Song, W.-P. Wang and W.-F. Zhang, *Appl. Phys. Lett.*, 2021, **119**, 042902.
74 T. C. U. Tromm, J. Zhang, J. Schubert, M. Luysberg, W. Zander, Q. Han, P. Meuffels, D. Meertens, S. Glass, P. Bernardy and S. Mantl, *Appl. Phys. Lett.*, 2017, **111**, 142904.
75 Z. Y. Quan, M. M. Wang, X. Zhang, H. H. Liu, W. Zhang and X. H. Xu, *AIP Adv.*, 2020, **10**, 085024.
76 S. Belahcen, T. Francois, L. Grenouillet, A. Bsiesy, J. Coignus and M. Bonvalot, *Appl. Phys. Lett.*, 2020, **117**, 252903.
77 Y. Sharma, D. Barrionuevo, R. Agarwal, S. P. Pavunny and R. S. Katiyar, *ECS Solid State Lett.*, 2015, **4**, N13–N16.
78 S. Starschich, D. Griesche, T. Schneller and U. Bottger, *ECS J. Solid State Sci. Technol.*, 2015, **4**, P419–P423.
79 H. Liu, S. Zheng, Q. Chen, B. Zeng, J. Jiang, Q. Peng, M. Liao and Y. Zhou, *J. Mater. Sci.: Mater. Electron.*, 2019, **30**, 5771–5779.
80 S. Zheng, Z. Zhao, Z. Liu, B. Zeng, L. Yin, Q. Peng, M. Liao and Y. Zhou, *Appl. Phys. Lett.*, 2020, **117**, 212904.
81 T. Schenk, N. Godard, A. Mahjoub, S. Girod, A. Matavz, V. Bobnar, E. Defay and S. Glinsek, *Phys. Status Solidi RRL*, 2020, **14**, 1900626.
82 S. J. Kim, D. Narayan, J.-G. Lee, J. Mohan, J. S. Lee, J. Lee, H. S. Kim, Y.-C. Byun, A. T. Lucero, C. D. Young, S. R. Summerfelt, T. San, L. Colombo and J. Kim, *Appl. Phys. Lett.*, 2017, **111**, 242901.
83 J. Müller, U. Schröder, T. S. Böscke, I. Müller, U. Bottger, L. Wilde, J. Sundqvist, M. Lemberger, P. Kücher, T. Mikolajick and L. Frey, *J. Appl. Phys.*, 2011, **110**, 114113.
84 T. Schenk, S. Mueller, U. Schroeder, R. Materlik, A. Kersch, M. Popovici, C. Adelmann, S. Van Elshocht, T. Mikolajick and I. Bucharest, ROMANIA, 2013, 260–263.
85 S. Starschich and U. Boettger, *J. Mater. Chem. C*, 2017, **5**, 333–338.
86 T. Shiraishi, S. Choi, T. Kiguchi, T. Shimizu, H. Uchida, H. Funakubo and T. J. Konno, *Jpn. J. Appl. Phys.*, 2018, **57**, 11UF02.
87 Y. F. Yao, D. Y. Zhou, S. D. Li, J. J. Wang, N. N. Sun, F. Liu and X. M. Zhao, *J. Appl. Phys.*, 2019, **126**, 8.
88 U. Schroeder, E. Yurchuk, J. Muller, D. Martin, T. Schenk, P. Polakowski, C. Adelmann, M. I. Popovici, S. V. Kalinin and T. Mikolajick, *Jpn. J. Appl. Phys.*, 2014, **53**, 85–89.
89 B. Ku, Y.-R. Jeon, M. Choi, C. Chung and C. Choi, *Appl. Surf. Sci.*, 2022, **601**, 154039.

 This journal is © The Royal Society of Chemistry 2024

Published on 29 November 2023. Downloaded by West Lake University on 2/18/2024 5:45:26 PM.

90 J. Muller, T. S. Boscke, U. Schroder, S. Mueller, D. Brauhaus, U. Bottger, L. Frey and T. Mikolajick, *Nano Lett.*, 2012, **12**, 4318–4323.
91 R. D. Shannon, *Acta Crystallogr., Sect. A: Cryst. Phys., Diffr., Theor. Gen. Crystallogr.*, 1976, **32**, 751–767.
92 T. S. Böscke, J. Müller, D. Bräuhaus, U. Schröder and U. Böttger, *Appl. Phys. Lett.*, 2011, **99**, 102903.
93 B. Xu, P. D. Lomenzo, A. Kersch, T. Mikolajick and U. Schroeder, *ACS Appl. Electron. Mater.*, 2022, **4**, 3648–3654.
94 Y. Feng, J. Wu, Q. Chi, W. Li, Y. Yu and W. Fei, *Chem. Rev.*, 2020, **120**, 1710–1787.
95 W. Dong, F. Tian, Q. Ma, D. Jiang, S. D. Seddon, A. E. Brunier, Z. Xia, S. U. H. Bakhtiar, L. Miao and Q. Fu, *Acta Mater.*, 2021, **213**, 116965.
96 W. Dong, W. Hu, T. J. Frankcombe, D. Chen, C. Zhou, Z. Fu, L. Cândido, G. Hai, H. Chen, Y. Li, R. L. Withers and Y. Liu, *J. Mater. Chem. A*, 2017, **5**, 5436–5441.
97 D. Wu, W. Dong, Y. Yang, L. Chen, W. Xiao, C. Zhang, K. Zou, W. Zhou, W. Luo, G. Zhang, Q. Fu and S. Jiang, *ACS Appl. Mater. Interfaces*, 2023, **15**, 14495–14501.
98 M. I. Popovici, A. M. Walke, J. Bizindavyi, J. Meersschaut, K. Banerjee, G. Potoms, K. Katcko, G. Van den Bosch, R. Delhougne, G. S. Kar and J. Van Houdt, *ACS Appl. Electron. Mater.*, 2022, **4**, 1823–1831.
99 P. D. Lomenzo, Q. Takmeel, C. Zhou, C.-C. Chung, S. Moghaddam, J. L. Jones and T. Nishida, *Appl. Phys. Lett.*, 2015, **107**, 242903.
100 N. Kaiser, Y.-J. Song, T. Vogel, E. Piros, T. Kim, P. Schreyer, S. Petzold, R. Valentí and L. Alff, *ACS Appl. Electron. Mater.*, 2023, **5**, 754–763.
101 L.-Y. Ma and S. Liu, *Phys. Rev. Lett.*, 2023, **130**, 096801.
102 J. Wei, L. Jiang, M. Huang, Y. Wu and S. Chen, *Adv. Funct. Mater.*, 2021, **31**, 2104913.
103 M. I. Popovici, J. Bizindavyi, P. Favia, S. Clima, M. N. K. Alam, R. K. Ramachandran, A. M. Walke, U. Celano, A. Leonhardt, S. Mukherjee, O. Richard, A. Illiberi, M. Givens, R. Delhougne, J. V. Houdt and G. S. Kar, *IEEE Int. Electron Devices Meet.*, 2022, 6.4.1–6.4.4.
104 F. Zhang, Z.-D. Luo, Q. Yang, J. Zhou, J. Wang, Z. Zhang, Q. Fan, Y. Peng, Z. Wu, F. Liu, S. Chen, D. He, H. Yin, G. Han, Y. Liu and Y. Hao, *ACS Appl. Mater. Interfaces*, 2022, **14**, 11028–11037.
105 B.-T. Lin, Y.-W. Lu, J. Shieh and M.-J. Chen, *J. Eur. Ceram. Soc.*, 2017, **37**, 1135–1139.
106 S. Starschich, T. Schenk, U. Schroeder and U. Boettger, *Appl. Phys. Lett.*, 2017, 110.
107 J. Wang, D. Zhou, W. Dong, X. Hou, F. Liu, N. Sun, F. Ali and Z. Li, *Ceram. Int.*, 2021, **47**, 16845–16851.
108 Z. Zou, G. Tian, D. Wang, Y. Zhang, J. Wang, Y. Li, R. Tao, Z. Fan, D. Chen, M. Zeng, X. Gao, J.-Y. Dai, X. Lu and J. M. Liu, *Nanotechnology*, 2021, **32**, 335704.
109 U. Schroeder, C. Richter, M. H. Park, T. Schenk, M. Pešić, M. Hoffmann, F. P. G. Fengler, D. Pohl, B. Rellinghaus, C. Zhou, C.-C. Chung, J. L. Jones and T. Mikolajick, *Inorg. Chem.*, 2018, **57**, 2752–2765.
110 S. T. Jaszewski, E. R. Hoglund, A. Costine, M. H. Weber, S. S. Fields, M. G. Sales, J. Vaidya, L. Bellcase, K. Loughlin, A. Salanova, D. A. Dickie, S. L. Wolfley, M. D. Henry, J.-P. Maria, J. L. Jones, N. Shukla, S. J. McDonnell, P. Reinke, P. E. Hopkins, J. M. Howe and J. F. Ihlefeld, *Acta Mater.*, 2022, **239**, 118220.
111 C. Palade, A.-M. Lepadatu, A. Slav, O. Cojocaru, A. Iuga, V. A. Maraloiu, A. Moldovan, M. Dinescu, V. S. Teodorescu, T. Stoica and M. L. Ciurea, *J. Mater. Chem. C*, 2021, **9**, 12353–12366.
112 M. Badillo, S. Taleb, T. Mokabber, J. Rieck, R. Castanedo, G. Torres, B. Noheda and M. Acuautla, *J. Mater. Chem. C*, 2023, **11**, 1119–1133.
113 L. Baumgarten, T. Szyjka, T. Mittmann, M. Materano, Y. Matveyev, C. Schlueter, T. Mikolajick, U. Schroeder and M. Muller, *Appl. Phys. Lett.*, 2021, **118**, 032903.
114 A. Pal, V. K. Narasimhan, S. Weeks, K. Littau, D. Pramanik and T. Chiang, *Appl. Phys. Lett.*, 2017, **110**, 022903.
115 T. Mittmann, M. Materano, P. D. Lomenzo, M. H. Park, I. Stolichnov, M. Cavalieri, C. Zhou, C.-C. Chung, J. L. Jones, T. Szyjka, M. Müller, A. Kersch, T. Mikolajick and U. Schroeder, *Adv. Mater. Interfaces*, 2019, **6**, 1900042.
116 J.-D. Luo, Y.-T. Yeh, Y.-Y. Lai, C.-F. Wu, H.-T. Chung, Y.-S. Li, K.-C. Chuang, W.-S. Li, P.-G. Chen, M.-H. Lee and H.-C. Cheng, *Vacuum*, 2020, **176**, 109317.
117 R. Hu, J. Tang, Y. Xi, Z. Jiang, Y. Lu, B. Gao, H. Qian and H. Wu, *IEEE Electron Device Lett.*, 2023, **44**, 618–621.
118 S.-N. Choi, S.-E. Moon and S.-M. Yoon, *Ceram. Int.*, 2019, **45**, 22642–22648.
119 H. Chen, Y. Chen, L. Tang, H. Luo, K. Zhou, X. Yuan and D. Zhang, *J. Mater. Chem. C*, 2020, **8**, 2820–2826.
120 G. Dearnaley, *Rep. Prog. Phys.*, 1969, **32**, 405.
121 S. Kang, W.-S. Jang, A. N. Morozovska, O. Kwon, Y. Jin, Y.-H. Kim, H. Bae, C. Wang, S.-H. Yang, A. Belianinov, S. Randolph, E. A. Eliseev, L. Collins, Y. Park, S. Jo, M.-H. Jung, K.-J. Go, H. W. Cho, S.-Y. Choi, J. H. Jang, S. Kim, H. Y. Jeong, J. Lee, O. S. Ovchinnikova, J. Heo, S. V. Kalinin, Y.-M. Kim and Y. Kim, *Science*, 2022, **376**, 731–738.
122 Y. Luo, C. Wang, C. Chen, Y. Gao, F. Sun, C. Li, X. Yin, C. Luo, U. Kentsch, X. Cai, M. Bai, Z. Fan, M. Qin, M. Zeng, J. Dai, G. Zhou, X. Lu, X. Lou, S. Zhou, X. Gao, D. Chen and J.-M. Liu, *Appl. Phys. Rev.*, 2023, **10**, 011403.
123 Y. Zhang, Y. Wang, Y. Wu, X. Shu, F. Zhang, H. Peng, S. Shen, N. Ogawa, J. Zhu and P. Yu, *Nat. Commun.*, 2023, **14**, 4012.
124 Z. Shen, H. Liu, Y. Shen, J. Hu, L. Chen and C. Nan, Machine learning in energy storage materials, *Interdiscip. Mater.*, 2022, **1**, 175–195.